

Research Article: New Research | Cognition and Behavior

The NeuroD6 subtype of VTA neurons contributes to psychostimulant sensitization and behavioral reinforcement

Zisis Bimpisidis¹, Niclas König¹, Stefanos Stagkourakis², Vivien Zell³, Bianca Vitek¹, Sylvie Dumas⁵, Bruno Giros^{6,7}, Christian Broberger², Thomas S. Hnasko^{3,4} and Åsa Wallén-Mackenzie¹

¹Department of Organismal Biology, Uppsala University, Uppsala, Sweden

²Department of Neuroscience, Karolinska Institutet, Stockholm, Sweden

³Department of Neurosciences, University of California, San Diego, La Jolla, USA

⁴Research Service VA San Diego Healthcare System, San Diego, CA 92161, USA

⁵Oramacell, Paris, France

⁶INSERM, UMRS 1130; CNRS, UMR 8246; Sorbonne University UPMC, Paris, France

⁷Douglas Mental Health University Institute & Department of Psychiatry, McGill University, Canada

<https://doi.org/10.1523/ENEURO.0066-19.2019>

Received: 22 February 2019

Revised: 7 May 2019

Accepted: 9 May 2019

Published: 16 May 2019

Author contributions: Z.B., S.S., V.Z., C.B., T.S.H., and x.W.-M. designed research; Z.B., N.K., S.S., V.Z., B.V., S.D., and x.W.-M. performed research; Z.B., N.K., S.S., V.Z., B.V., S.D., C.B., T.S.H., and x.W.-M. analyzed data; Z.B. and x.W.-M. wrote the paper; B.G. contributed unpublished reagents/analytic tools.

Funding: hjärnfonden

;

Funding: vetenskapsrådet

.

Conflict of Interest: Author Sylvie Dumas is the owner of Oramacell. All other authors declare no competing interests.

Work in ÅWM lab was supported by Uppsala University, Vetenskapsrådet (MH), Hjärnfonden, Parkinsonfonden, the Research Foundations of Bertil Hällsten and Åhlén. Work in CB lab was supported by Vetenskapsrådet (MH), the European Research Council, Novo Nordisk Fonden and the Strategic Research Programme for Diabetes Research at Karolinska Institutet. Work in TSH lab was supported by NIH DA036612 and VA BX003759.

Correspondence should be addressed to Åsa Wallén-Mackenzie at asa.mackenzie@ebc.uu.se.

Cite as: eNeuro 2019; 10.1523/ENEURO.0066-19.2019

Alerts: Sign up at www.eneuro.org/alerts to receive customized email alerts when the fully formatted version of this article is published.

Accepted manuscripts are peer-reviewed but have not been through the copyediting, formatting, or proofreading process.

Copyright © 2019 Bimpisidis et al.

This is an open-access article distributed under the terms of the Creative Commons Attribution 4.0 International license, which permits unrestricted use, distribution and reproduction in any medium provided that the original work is properly attributed.

1 1. Manuscript Title (50 word maximum)

2

3 **The NeuroD6 subtype of VTA neurons contributes to psychostimulant sensitization and**
4 **behavioral reinforcement**

5

6 2. Abbreviated Title (50 character maximum)

7

8 NeuroD6 VTA neurons in reward-related behavior

9

10 3. List all Author Names and Affiliations in order as they would appear in the published
11 article

12

13 Zisis Bimpisidis¹, Niclas König¹, Stefanos Stagkourakis², Vivien Zell³, Bianca Vlcek¹, Sylvie

14

14 Dumas⁵, Bruno Giros^{6,7}, Christian Broberger², Thomas S. Hnasko^{3,4}, Åsa Wallén-Mackenzie^{1*}

15

16 ¹Department of Organismal Biology, Uppsala University, Uppsala, Sweden

17 ²Department of Neuroscience, Karolinska Institutet, Stockholm, Sweden

18 ³Department of Neurosciences, University of California, San Diego, La Jolla, USA

19 ⁴Research Service VA San Diego Healthcare System, San Diego, CA 92161, USA

20 ⁵Oramacell, Paris, France

21 ⁶INSERM, UMRS 1130; CNRS, UMR 8246; Sorbonne University UPMC, Paris, France

22 ⁷Douglas Mental Health University Institute & Department of Psychiatry, McGill University,
23 Canada.

24

25 4. Author Contributions:

26

27 ZB planned experiments, performed histological and behavioral experiments, analyzed data,

28 prepared figures, wrote the manuscript; NK planned experiments, performed behavioral

29 experiments, analyzed data, prepared figures; SS planned, performed, analyzed FSCV

30 experiments, prepared figures; VZ, planned, performed, analyzed patch clamp experiments,

31 prepared figures; BV performed histological experiments, analyzed data; SD planned and

32 performed histological experiments, prepared figures; BG produced and contributed
33 *Vmat2^{lox/lox}* mice; CB planned FSCV experiments and analyzed data; TSH planned patch
34 clamp experiments and analyzed data; ÅWM, conceived and planned all experiments,
35 analyzed data, wrote the manuscript.

36
37 5. Correspondence should be addressed to (include email address)

38
39 Åsa Wallén-Mackenzie. E-mail: asa.mackenzie@ebc.uu.se

40
41
42 6. Number of Figures 10

43
44
45 7. Number of Tables 2

46
47
48 8. Number of Multimedia 0

49
50
51 9. Number of words for Abstract 249

52
53
54 10. Number of words for Significance Statement 111

55
56
57 11. Number of words for Introduction 750

58
59
60 12. Number of words for Discussion 1969

61
62
63 13. Acknowledgements

64
65 Professors Lars Olson and Nils-Göran Larsson (Karolinska Institutet, Sweden) are thanked for
66 the DAT-Cre transgenic mice, Professor Ole Kiehn (Karolinska Institutet, Sweden and
67 University of Copenhagen, Denmark) for the Vglut2-Cre mice and Prof Klaus-Armin Nave
68 and Dr Sandra Goebbels (Max Planck Institute of Experimental Medicine, Göttingen,
69 Germany) for the NEX-Cre mice. BioVis (Uppsala University) and Image platform at
70 Institute de la Vision (Paris, France) are thanked for slide scanning. Current and previous

71 members of the Mackenzie lab are thanked for technical assistance and constructive
72 comments.

73

74 14. Conflict of Interest

75

76 Author Sylvie Dumas is the owner of Oramacell.

77 All other authors declare no competing interests.

78

79 15. Funding sources

80

81 Work in ÅWM lab was supported by Uppsala University, Vetenskapsrådet (MH),

82 Hjärnfonden, Parkinsonfonden, the Research Foundations of Bertil Hällsten and Åhlén. Work

83 in CB lab was supported by Vetenskapsrådet (MH), the European Research Council, Novo

84 Nordisk Fonden and the Strategic Research Programme for Diabetes Research at Karolinska

85 Institutet. Work in TSH lab was supported by NIH DA036612 and VA BX003759.

86

87

88

89

90

91

92

93

94

95

96 **The NeuroD6 subtype of VTA neurons contributes to psychostimulant sensitization and**
97 **behavioral reinforcement**

98 *Short title:* NeuroD6 VTA neurons in reward-related behavior

99 **Abstract**

100 Reward-related behavior is complex and its dysfunction correlated with neuropsychiatric
101 illness. Dopamine neurons of the ventral tegmental area (VTA) have long been associated
102 with different aspects of reward function, but it remains to be disentangled how distinct VTA
103 dopamine neurons contribute to the full range of behaviors ascribed to the VTA. Here, a
104 recently identified subtype of VTA neurons molecularly defined by NeuroD6 (NEX1M) was
105 addressed. Among all VTA dopamine neurons, less than 15% were identified as positive for
106 NeuroD6. In addition to dopaminergic markers, sparse NeuroD6 neurons expressed the
107 *Vesicular glutamate transporter 2* gene. To achieve manipulation of NeuroD6 VTA neurons,
108 NeuroD6(NEX)-Cre-driven mouse genetics and optogenetics were implemented. First,
109 expression of *Vesicular monoamine transporter 2* was ablated to disrupt dopaminergic
110 function in NeuroD6 VTA neurons. Comparing *Vmat2*^{lox/lox;NEX-Cre} conditional knockout
111 (cKO) mice with littermate controls, it was evident that baseline locomotion, preference for
112 sugar and ethanol, and place preference upon amphetamine- and cocaine-induced
113 conditioning were similar between genotypes. However, locomotion upon repeated
114 psychostimulant administration was significantly elevated above control level in cKO mice.
115 Second, optogenetic activation of NEX-Cre VTA neurons was shown to induce dopamine
116 release and glutamatergic post-synaptic currents within the nucleus accumbens. Third,
117 optogenetic stimulation of NEX-Cre VTA neurons *in vivo* induced significant place
118 preference behavior, while stimulation of VTA neurons defined by Calretinin failed to cause a
119 similar response. The results show that NeuroD6 VTA neurons exert distinct regulation over

120 specific aspects of reward-related behavior, findings that contribute to the current
121 understanding of VTA neurocircuitry.

122 **Significance statement**

123 Reward-related behavior is complex and its dysfunction is implicated in many
124 neuropsychiatric disorders, including drug addiction. Midbrain dopamine neurons of the
125 ventral tegmental area (VTA) are crucial for reward behavior, but due to recently uncovered
126 heterogeneity, it remains to be fully resolved how they regulate reward responsiveness and
127 how their dysfunction might contribute to disease. Here we show that the recently described
128 NeuroD6 (NEX) subtype of VTA dopamine neurons is involved in psychostimulant
129 sensitization and that optogenetic stimulation of NEX-Cre VTA neurons induces dopamine
130 release, glutamatergic post-synaptic currents and real time place preference behavior.
131 NeuroD6 VTA neurons thus exert distinct regulation over specific aspects of reward-related
132 behavior, findings that contribute to the current understanding of VTA neurocircuitry.

133

134 **Introduction**

135 The midbrain dopamine (mDA) system mediates a diverse spectrum of behaviors and their
136 dysfunction is correlated with a range of severe behavioral disorders including substance use
137 disorder, schizophrenia, ADHD and Parkinson's disease (PD). Consequently, therapies based
138 on modulating the activity of the mDA system are commonly prescribed, however, due to
139 their unselective nature, current treatments often fail to alleviate symptoms and instead cause
140 adverse effects (Divac et al., 2014; Weintraub, 2008). One reason for the lack of successful
141 treatment is incomplete understanding of the underlying neurobiology. Indeed, it is
142 increasingly understood that the mDA system is highly heterogeneous (reviewed in Morales
143 and Margolis, 2017; Pupe and Wallén-Mackenzie, 2015). Beyond the classical separation into

144 the ventral tegmental area (VTA) and substantia nigra *pars compacta* (SNc), with VTA
145 projections to cortical and limbic target areas and SNc projections to the dorsal striatum
146 subserving cognitive/affective and motor functions, respectively (Björklund and Dunnett,
147 2007), a higher level of complexity is now being unfolded: Afferent and efferent projections,
148 electrophysiological patterns, capacity for glutamate or GABA co-release and responsiveness
149 to appetitive or aversive stimuli are some of the properties that distinguish mDA neurons from
150 each other (Beier et al., 2015; Faget et al., 2016; Lammel et al., 2011; Menegas et al., 2015).

151

152 Likely coupled to this functional diversity is a complex diversity in molecular identity.
153 Microarray-based analyses have identified gene expression patterns enriched in VTA over
154 SNc DA neurons (Chung et al., 2005; Greene et al., 2005; Viereckel et al., 2016) while single
155 cell profiling has begun to identify combinatorial gene expression patterns that molecularly
156 define subtypes of mDA neurons (Hook et al., 2018; La Manno et al., 2016; Poulin et al.,
157 2014). Based on this new knowledge, intersectional genetic approaches were recently
158 described in which the distinct projection pathways of several newly defined subtypes of
159 mDA neurons were identified (Poulin et al., 2018). By forwarding the current knowledge
160 towards molecularly defined, and thus targetable, subtypes of mDA neurons with distinct
161 projection patterns, these recent advances enhance the possibility of improving selectivity in
162 treatment of dopaminergic disorders. However, a key issue that remains to be resolved is how
163 each molecularly defined subtype of DA neuron contributes to the complex range of
164 behaviors ascribed to the mDA system.

165 The gene encoding the transcription factor NeuroD6 (aka NEX1M) has recently gained
166 attention due to its selective expression within subsets of VTA DA neurons while being
167 excluded from the SNc (Khan et al., 2017; Kramer et al., 2018; Viereckel et al., 2016). VTA
168 DA neurons are of particular interest for several reasons. First, the importance of VTA DA

169 neurons in several aspects of behavioral reinforcement and conditioning has been established
170 through classical studies (reviewed in Di Chiara and Bassareo, 2007; Ikemoto, 2007), and
171 more recently, by the use of optogenetics (Ilango et al., 2014; Kim et al., 2012; Pascoli et al.,
172 2015; Tsai et al., 2009). However, detailed knowledge of the exact nature of those particular
173 DA neurons that contribute to each of these complex behaviors remains elusive. Second,
174 medial DA neurons mediate the most potent responsiveness to addictive drugs via their
175 projection to the nucleus accumbens shell (NAcSh) (Ikemoto and Bonci, 2014). The
176 possibility to ascribe specific aspects of drug responses to a distinct subtype of VTA DA
177 neurons would therefore enhance the understanding of addictive behavior. Third, certain VTA
178 neurons show resistance to degeneration in PD (Brichta and Greengard, 2014), however,
179 depending on their role in behavioral regulation, surviving VTA neurons might contribute to
180 non-motor symptoms including behavioral addictions (Cenci et al., 2015).

181 While *NeuroD6*-expressing DA neurons were recently identified as neuroprotected in
182 experimental PD (Kramer et al., 2018), the potential role of this newly described subtype of
183 VTA neurons in behavioral regulation has remained unexplored. Here, we implemented
184 *NeuroD6-Cre* mice (*aka* NEX-Cre) to create opportunities for targeting and manipulation of
185 the *NeuroD6* subtype VTA neurons. We show that gene targeting of Vesicular monoamine
186 transporter 2 (VMAT2) within this particular DA neuron subtype elevated the locomotor
187 response to psychostimulants while activation of *NeuroD6-Cre* neurons by optogenetic
188 stimulation in the medial VTA induced DA release and glutamatergic post-synaptic responses
189 in the NAcSh. *In vivo* optogenetic activation of the *NeuroD6-Cre* VTA subpopulation in a
190 real-time place preference failed to trigger a conditioned response but induced place
191 preference upon direct stimulation. These results advance the current understanding of the
192 VTA circuitry by identifying discrete aspects of reward-related behavior correlated with the
193 *NeuroD6* subtype VTA neurons.

194 **Materials and Methods**

195 **Mice**

196 Mice were provided with food and water *ad libitum* and housed according to Swedish
197 legislation (Animal Welfare Act SFS 1998:56) and European Union legislation (Convention
198 ETS 123 and Directive 2010/63/EU). Mice of either sex were used. Experiments were
199 conducted with permission from the local Animal Ethical Committees. DAT-Cre (Ekstrand et
200 al., 2007), Vglut2-Cre (Borgius et al., 2010), Calb2-Cre (Jackson laboratory,
201 RRID:MGI_4365741) and NeuroD6-Cre/NEX-Cre (Goebbels et al., 2006) transgenic mice
202 were bred with C57BL/6N Tac wildtype mice (Taconic) for optogenetics-based experiments.
203 NEX-Cre mice were also bred with *Vmat2*^{lox/lox} mice, in which exon 2 of the *Vmat2* gene is
204 flanked by LoxP sites (Narboux-Nême et al., 2011) to generate conditional knockout
205 (*Vmat2*^{lox/lox;NEX-Cre-tg}: cKO) mice in which *Vmat2* exon 2 is ablated upon NEX-Cre-mediated
206 recombination of LoxP sites. Littermate mice negative for the NEX-Cre-transgene served as
207 control mice (*Vmat2*^{lox/lox;NEX-Cre-wt}: Ctrl) (illustrated in Fig. 2A). Mice were genotyped by PCR
208 using the following primer sequences: Cre (applies to DAT-Cre, NEX-Cre, and Calb2-Cre):
209 5'-ACG AGT GAT GAG GTT CGC AAG A-3'; 5'-ACC GAC GAT GAA GCA TGT TTA
210 G-3'; Vglut2-Cre: 5'-TTG CAT CGC ATT GTC TGA GTA G-3'; 5'-TTC CCA CAC AAG
211 ATA CAG ACT CC-3'; Vmat2Lox: 5'-GAC TCA GGG CAG CAC AAA TCT CC-3'; 5'-
212 GAA ACA TGA AGG ACA ACT GGG ACC C-3'.

213

214 ***In situ* hybridization**

215 *In situ* hybridization (ISH) using radioactive oligoprobes

216 The following probes sequences were used:

217 NeuroD6: NM_009717.2; bases 99-132, 933-966, 1256-1288

218 Th: NM_009377.1; bases 774-807, 272-305, 1621-1655

219 Vmat2exon1: NM_172523.3; bases18-51 and 83-116

220 Vmat2exon2: NM_172523.3; bases 201-237 and 240-276

221 Oligoprobes were 3' end-labeled with [alpha-³⁵S]dATP using terminal deoxynucleotidyl
222 transferase at a specific activity of 5x10⁸ d.p.m./μg. Sections were fixed in 3.7 %
223 formaldehyde in phosphate-buffered saline (PBS) for 1 h, washed in PBS, rinsed in water,
224 dehydrated in 70 % ethanol and air-dried. Hybridization was carried out at 42 °C for 16 h in
225 hybridization medium (Oramacell, France) containing the labeled antisense oligonucleotides
226 (3.10⁵ cpm / 100 μl). Sections were washed to a final stringency of 0.5 SSC at 53 °C,
227 dehydrated in ethanol, air-dried and exposed to Fujifilm BioImaging Analyzer BAS-5000 for
228 15 days.

229

230 Double and triple *in situ* hybridization using riboprobes (fluorescent *in situ* hybridization
231 (FISH) or combined FISH /brightfield *in situ* hybridization (FISH/ISH))

232 The following probes sequences were used:

233 Calb2: NM_007586.1; bases 80-793

234 Dat (Slc6a3): NM_012694.2; bases 1015-1938

235 NeuroD6: NM_009717.2; bases 635-1419

236 Th: NM_009377.1; bases 456-1453

237 Vglut2 (Slc17a6): NM_080853.3; bases 2315-3244

238 Viaat (Slc32a1): NM_009508.2; bases 649-1488

239 Vmat 2 Probe 1: Vmat2: NM_0130331.1 (rat); bases 701-1439 (corresponds to exon 6-15 of
240 mouse sequence NM_172523.3)

241 Vmat2 Probe 2: NM_172523.3; bases142-274 i.e. the whole exon 2

242 Detection of Th, Dat, Vglut2, Viaat, Calb2, NeuroD6 mRNA and Vmat2 Probe 1 and Probe 2
243 mRNA in brain tissue using *in situ* hybridization was performed following a previously

244 published protocol (Viereckel et al., 2016). Briefly, mice were sacrificed and brains dissected.
245 Coronal cryosections were prepared, air-dried, fixed in 4% paraformaldehyde and acetylated
246 in 0.25% acetic anhydride/100 mM triethanolamine (pH=8) followed by hybridization for 18h
247 at 65 °C in 100 µl of formamide-buffer containing 1 µg/ml digoxigenin (DIG)-labeled probe
248 for colorimetric detection or 1 µg/ml DIG- or 1 µg/ml fluorescein-labeled probes for
249 fluorescent detection. Sections were washed at 65 °C with SSC buffers of decreasing strength,
250 and blocked with 20% FBS and 1% blocking solution. For colorimetric detection, DIG
251 epitopes were detected with alkaline phosphatase-coupled anti-DIG fab fragments at 1/500
252 and signal developed with NBT/BCIP. For fluorescent detection, sections were incubated
253 with HRP-conjugated anti-fluorescein antibody at 1/1000 concentration (Roche
254 Cat#11426346910, RRID:AB_840257). Signals were revealed with the TSA™ Kit (Perkin
255 Elmer Cat# NEL749A001KT) using biotin-tyramide at 1:75 concentration followed by
256 incubation with neutravidin Oregon Green conjugate at 1:750 (Molecular Probes Cat#A-6374,
257 RRID:AB_2315961). HRP-activity was stopped by incubation of sections in 0,1 M glycine
258 and 3% H₂O₂. DIG epitopes were detected with HRP conjugated anti-DIG antibody at 1:1000
259 (Roche Cat#11207733910, RRID:AB_514500) and revealed with TSA™ Kit (Perkin Elmer
260 Cat# NEL744A001KT) using Cy3 tyramide at 1:200. For triple FISH, TH mRNA was
261 detected with Dinitrophenyl (DNP)-labeled probe; NeuroD6 mRNA with DIG-labeled
262 probe and Vglut2 mRNA with fluorescein-labeled probe. The protocol was the same as
263 described above until revelation: DIG epitopes were detected with HRP anti-DIG fab
264 fragments at 1:3000 and revealed using Cy3 tyramide at 1:50 followed by glycine and H₂O₂
265 treatment. Fluorescein epitopes were detected with HRP anti-fluorescein fab fragments at
266 1:5000 and revealed using Cy2-tyramide at 1:250 by glycine and H₂O₂ treatment. DNP
267 epitopes were detected with HRP anti-DNP fab fragments at 1:1000 and revealed using Cy5-
268 tyramide at 1:50, followed by incubation with DAPI. Fluorophore-tyramides were synthesized

269 as previously described (Hopman et al., 1998). All slides were scanned and analyzed on
270 NanoZoomer 2.0-HT Ndp2.view (Hamamatsu). Stereotaxic reference atlases (Franklin and
271 Paxinos, 2008; Fu et al., 2012) were used to outline anatomical borders.

272

273 Validation of NEX-Cre-mediated recombination of floxed *Vmat2* exon 2

274 Upon genotyping, PCR-validated *Vmat2*^{lox/lox;NEX-Cre-*tg*} (cKO) and *Vmat2*^{lox/lox;NEX-Cre-*wt*} (Ctrl)
275 mice were sacrificed and brains analyzed by *in situ* hybridization to verify NEX-Cre-driven
276 recombination of the floxed exon 2 of the *Vmat2* gene in cKO mice. Littermate Ctrl mice
277 were used to validate wildtype *Vmat2* mRNA. A *Vmat2* mRNA 2-probe approach was
278 implemented to visualize cells positive for wildtype *Vmat2* mRNA and cells positive for a
279 truncated *Vmat2* mRNA generated upon NEX-Cre-driven recombination of the floxed *Vmat2*
280 exon 2. Probe 1 (green) was designed for detection of *Vmat2* mRNA derived from exon 6-15
281 and Probe 2 (blue) for detection of mRNA from exon 2 (illustrated in Fig. 2B). In control
282 mice, both Probe 1 and Probe 2 can bind their target mRNA (wildtype *Vmat2* mRNA).
283 Combination of Probe 1 and Probe 2 gives rise to combined blue and green labeling in
284 wildtype DA neurons. In cKO mice, *Vmat2* exon 2 will be deleted specifically in cells
285 expressing the NEX-Cre transgene, leading to production of *Vmat2* mRNA missing exon 2
286 but maintaining exons 6-15. In *Vmat2*-expressing cells that do not express the NEX-
287 Cre transgene in cKO mice, wildtype *Vmat2* mRNA will be produced. *Vmat2*-targeted cells
288 can thus be identified based on lack of blue color (Probe 2) and presence of green color only
289 (Probe 1). Thus, using the *Vmat2* mRNA 2-probe-approach, the color shift from complete
290 overlap of blue and green color in Ctrl mice to the presence of green-only cells in cKO mice
291 is used to verify Cre-LoxP-mediated conditional knockout of the *Vmat2* gene.

292

293 **Immunohistochemistry**

294 Detection of TH and eYFP proteins took place according to standard immunohistochemical
295 protocols using primary antibodies [mouse anti-TH (1:1000, Millipore Cat# MAB318,
296 RRID:AB_2201528), chicken anti-GFP (1:1000, Abcam Cat# ab13970, RRID:AB_300798)].
297 After overnight incubation, primary antibodies were removed and sections were incubated in
298 specific fluorophore-conjugated secondary antibodies (donkey anti-mouse Cy3, Millipore
299 Cat#AP192C, RRID:AB_11214096, donkey anti-chicken A488, Jackson ImmunoResearch
300 Labs Cat# 703-545-155, RRID:AB_2340375, both 1:500). Upon rinses, slides were
301 coverslipped using Fluoromount Aqueous mounting medium (Sigma-Aldrich Cat# F4680).
302 For bright-field detection of TH, the peroxidase-based method (ABC-kit; Vector Laboratories
303 Cat# PK-4001, RRID:AB_2336810) with DAB chromogen was used. Quantifications were
304 done manually on 3 mice per group. A stereotaxic atlas (Franklin and Paxinos, 2008) was
305 used to outline anatomical borders.

306

307 **Behavioral analysis**

308 *Vmat2*^{lox/lox;NEX-Cre-tg} cKO and *Vmat2*^{lox/lox;NEX-Cre-wt} Ctrl mice were analyzed in the following
309 behavioral tests:

310 Baseline locomotion

311 Spontaneous locomotion and habituation in a novel environment were monitored for 30 min
312 upon placing the mice in Makrolon® polycarbonate boxes containing 1.5 cm bedding and a
313 transparent plexiglas lid. Locomotor behavior of the mice was recorded by the EthovisionXT
314 software (Noldus, RRID:SCR_000441).

315 Sucrose preference test

316 Preference to sucrose was assessed in the home cage of the mice. The mice were housed
317 individually in cages containing two drinking bottles. After 48h of habituation to the
318 experimental set up, they were presented to one bottle of tap water and one of sucrose

319 solution (1, 3 and 10%) that were replaced and weighted every 24h. Each concentration was
320 tested twice and the position of the bottles was alternated to avoid side bias.

321 Ethanol preference test

322 Individually housed mice had access to one bottle of tap water and one of alcohol solution (3,
323 6 and 10%) that were replaced and weighted every 24h. Each concentration of ethanol was
324 tested four times.

325 Cocaine-induced locomotion

326 Mice were placed in Makrolon® polycarbonate boxes containing 1.5cm bedding and a
327 transparent plexiglass lid and their locomotor behavior was recorded 30 min pre- and 60 min
328 post-injection of saline or cocaine injections (5, 10 & 20 mg/kg, i.p.) on four consecutive
329 days. Locomotor behavior of the mice was recorded by the EthovisionXT software (Noldus,
330 RRID:SCR_000441).

331 Amphetamine sensitization

332 Upon habituation, mice received a saline injection (Day 1) followed by 4 days of
333 amphetamine injections (Days 2-5, 3 mg/kg, i.p.) followed by a last injection on Day 17.
334 Locomotion was recorded 30 min pre- and 1.5 h post-injection. Locomotor behavior of the
335 mice was recorded by the EthovisionXT software (Noldus, RRID:SCR_000441).

336 Conditioned-placed preference (CPP)

337 An apparatus (Panlab, Harvard Apparatus) consisting of two-main compartments [20cm (W)
338 x 18cm (L) x 25cm (H)] with distinct wall and floor texture patterns and one connecting,
339 transparent compartment [20cm (W) x 7cm (L) x 25cm (H)]. The CPP procedure was
340 conducted throughout six days. Firstly, during the Pre-test, the mice were placed in the
341 apparatus and left to freely explore. This session was used to assess initial preferences and to
342 calculate the preference score (see below). During the next four consecutive conditioning
343 days, the mice were constrained in one of the two main compartments and received drug

344 injections (cocaine, 20 mg/kg or amphetamine, 3 mg/kg, i.p.) in the least preferred
345 compartment or saline injections in the opposite one. The conditioning sessions were repeated
346 twice a day [morning (a.m); afternoon (p.m)] and the treatment was alternated between days.
347 Thus, the mice received in total 4 injections of saline and 4 injections of the drug,
348 counterbalanced between sessions and genotypes. On the Test day, the mice were placed
349 again in the apparatus and were let to freely explore. The preference score was calculated by
350 subtracting the time in seconds the animal spent in the drug-paired compartment during pre-
351 test from the time spent in the same compartment during the test (Δ Sec). All sessions lasted
352 30 minutes and the locomotor behavior of the mice was recorded by the EthovisionXT
353 software (Noldus, RRID:SCR_000441).

354

355 **Stereotaxic injections**

356 Optogenetic viruses were purchased from University of North Carolina, Vector Core, US.
357 DAT-Cre, Vglut2-Cre, Calb2-Cre and NEX-Cre mice (>8 weeks; >20g) were deeply
358 anesthetized with isoflurane and received infusions of 300nl of *AAV5-EF1a-DIO-*
359 *ChR2(H134)-eYFP* or *AAV5-EF1a-DIO-eYFP-WPREpA* in the right VTA (AP: -3.45 mm, L:
360 -0.2 mm, V: -4.4 mm according to (Franklin and Paxinos, 2008) at 100 nl min⁻¹ flow rate. For
361 behavioral analysis, an optic fiber was implanted and stabilized above the right VTA (AP: -
362 3.4 mm, ML: -0.3 mm, DV: -4.0mm) using anchor screws and dental cement. A subset of
363 NEX-Cre mice was injected bilaterally with *AAV5-EF1a-DIO-ChR2(H134)-eYFP* before
364 fiber implantation. After post-mortem histological analysis, mice with limited transfection in
365 the VTA and/or misplaced optic fiber were excluded from statistical analysis.

366

367 **Imaging, cell counting and analysis of projection target areas**

368 Quantification of *in situ* hybridization. Manual counting of cells expressing mRNAs of
369 interest was performed in 2-3 mice per probe pair with Th mRNA as reference for outline of
370 the VTA and Th, Dat, Viaat or Vglut2 mRNA as reference for distinct cell soma. A signal for
371 a particular mRNA was considered as specific for a particular cell when five contiguous
372 fluorescent dots were present within the outline of the cell soma.

373 Quantification of immunohistochemistry. Sections of Calb2-Cre and NEX-Cre mice injected
374 with *AAV5-EF1a-DIO-ChR2(H134)-eYFP* containing the VTA (-3.28 mm to -3.80 mm from
375 bregma according to Franklin and Paxinos, 2008) were immunostained for eYFP and TH as
376 described above. Z-stacks in 4 different positions within the VTA, representative of subareas
377 (VTA1-VTA4 of which VTA1 and VTA3 represented medial VTA and VTA2 and VTA4
378 lateral VTA on two different bregma levels, Fig. 5G), were acquired using a Zeiss Confocal
379 microscope (LSM 700, 20x magnification). Co-labeling of YFP and TH was identified for
380 each fluorescent channel and counted manually using the ImageJ software
381 (RRID:SCR_003070). A minimum of 3 mice of each genotype was processed and analyzed.

382 Analysis of projection areas. Fluorescent microscopy (Zeiss Confocal microscope) was used
383 to detect eYFP-positive fibers in sections derived from the whole brain of NEX-Cre, Calb2-
384 Cre, DAT-Cre and NEX-Cre mice injected into the VTA with *AAV5-EF1a-DIO-*
385 *ChR2(H134)-eYFP*. A minimum of 2 mice of each genotype was analyzed by 2 persons blind
386 to the genotype of the mice.

387

388 **Fast-scan cyclic voltammetry in slices**

389 For DA recordings in terminal areas upon photostimulation, DAT-Cre, Calb2-Cre and NEX-
390 Cre mice were injected with *AAV5-EF1a-DIO-ChR2(H134)-eYFP* or *AAV5-EF1a-DIO-*
391 *eYFP-WPREpA* as described above.

392 Carbon Fiber Microelectrodes. Carbon fiber working electrodes were fabricated by aspirating
393 7 μm diameter carbon fibers (Cytac engineered materials, Tempe, AZ) into borosilicate glass
394 capillaries (1.2 mm O.D., 0.69 mm I.D., Sutter Instrument Co, CA). Capillaries were adjusted
395 (Sutter Instrument, P-97) and sealed with epoxy (EpoTek 301, Epoxy Technology, MA).
396 Electrodes were tested on bath applications of known concentrations of DA. Only electrodes
397 showing good reaction kinetics (current vs time plots, and current vs voltage plots) were used.
398 Fast-scan cyclic voltammetry (FSCV). A Dagan Chem-Clamp potentiostat (Dagan
399 Corporation, MN) and two data acquisition boards (PCI-6221, National Instruments, TX) run
400 by the TH 1.0 CV program (ESA, MA) were used to collect all electrochemical data. Cyclic
401 voltammograms were obtained by applying a triangular waveform potential (-0.4 to $+1.3$ V
402 vs Ag/AgCl) repeated every 100 ms at a scan rate of 200 V/s (low pass Bessel filter at 3 kHz).
403 Each cyclic voltammogram was a background-subtracted average of 10 successive cyclic
404 voltammograms taken at the maximum oxidation peak current. All electrodes were allowed to
405 cycle for at least 15 min before recording to stabilize the background current. The recorded
406 current response was converted to DA concentration via *in vitro* electrode calibration with
407 standard DA solution after each experiment. For optically evoked DA release,
408 photostimulation during FSCV recordings was generated through a 3.4 Watt 447 nm LED
409 mounted on the microscope oculars and delivered through the objective lens.
410 Photostimulation was controlled via a DigiData 1440A, enabling control over duration and
411 intensity. Illumination intensity typically scaled to 3 mW/mm^2 . Acquired data were analysed
412 and plotted using Matlab (RRID:SCR_001622) routines and statistical analysis was
413 performed using Prism 6.0 (GraphPad Software, La Jolla, CA, RRID:SCR_002798)

414

415 **Patch-clamp electrophysiology in slices**

416 For recordings of excitatory post synaptic currents (EPSCs) and inhibitory post synaptic
417 currents (IPSCs) upon optogenetic stimulation, Calb2-Cre and NEX-Cre mice (>8 weeks, >20
418 g) were injected with *AAV5-EF1a-DIO-ChR2(H134R)-eYFP* as described above. Mice were
419 deeply anaesthetized with pentobarbital (200 mg.kg⁻¹ i.p.; Virbac) and perfused intracardially
420 with 10 ml ice-cold sucrose-artificial cerebrospinal fluid (ACSF) containing (in mM): 75
421 sucrose, 87 NaCl, 2.5 KCl, 7 MgCl₂, 0.5 CaCl₂, 1.25 NaH₂PO₄, 25 NaHCO₃ and continuously
422 bubbled with carbogen (95% O₂-5% CO₂). 200 µm coronal brain slices were cut in sucrose-
423 ACSF. Slices were transferred to a perfusion chamber containing ACSF at 31 °C (in mM):
424 126 NaCl, 2.5 KCl, 1.2 MgCl₂, 2.4 CaCl₂, 1.4 NaH₂PO₄, 25 NaHCO₃, 11 glucose,
425 continuously bubbled with carbogen. After at least 45 min recovery, slices were transferred to
426 a recording chamber continuously perfused with ACSF (2–3 ml min⁻¹) maintained at 29–31
427 °C. Patch pipettes (3.5–5.5 MΩ) were pulled from borosilicate glass and filled with internal
428 recording solution containing (in mM): 120 CsCH₃SO₃, 20 HEPES, 0.4 EGTA, 2.8 NaCl, 5
429 TEA, 2.5 Mg-ATP, 0.25 Na-GTP, at pH 7.25 and 285 ± 5 mOsm. VTA neurons and terminals
430 were visualized by epifluorescence and visually guided patch recordings were achieved using
431 infrared differential interference contrast (IR-DIC) illumination (Axiocam MRm, Zeiss).
432 ChR2 was activated by flashing blue light (5-ms pulse width) through the light path of the
433 microscope using a light-emitting diode (UHP-LED460, Prizmatix) under computer control.
434 EPSCs and IPSCs were recorded in whole-cell voltage clamp (-60 mV and 0mV holding
435 potential respectively, Multiclamp 700B amplifier, Axon Instruments), filtered at 2 KHz,
436 digitized at 10 KHz (Axon Digidata 1550, Axon Instruments), and collected online using
437 pClamp 10 software (Molecular Device). Series resistance and capacitance were
438 electronically compensated before recordings. Estimated liquid-junction potential was 12mV
439 and left uncorrected. Series resistance and/or leak current were monitored during recordings
440 and cells that showed >25% change during recordings were considered unstable and

441 discarded. Single-pulse (5-ms) photostimuli were applied every 55 s and 10 photo-evoked
442 currents were averaged per neuron per condition. DMSO stock solution of 6,7-
443 dinitroquinoxaline-2,3-dione (DNQX, 10 mM, Sigma) was diluted 1,000-fold in ACSF and
444 bath applied. Current sizes were calculated by using peak amplitude from baseline. Decay
445 time constants (τ) were calculated by fitting an exponential function to each averaged current
446 trace using the following formula: $f(t)=e^{-t/\tau} + C$.

447

448 **Place preference upon optogenetic stimulation**

449 The three-compartment apparatus (Panlab, Harvard Apparatus) used in the CPP experiments
450 (above) was also implemented in the optogenetics-driven place preference experiments to
451 address real time place preference upon photostimulation (RT-PP) and conditioned response
452 (CR), the association to compartment previously paired with photostimulation. Similar to
453 protocols previously described by others (Qi et al., 2016; Root et al., 2014), the entry of the
454 mouse into one of the two main compartments was paired with intracranial VTA
455 photostimulation (10 ms pulse width, 20 Hz, 10 mW) while the interconnecting compartment
456 was not coupled to light stimulation (neutral) at all. The EthovisionXT tracking software
457 (Noldus, RRID:SCR_000441) was used to monitor behavior and trigger laser stimulation.
458 Behavior was assessed over the course of 8 experimental days (Fig. 8A) subdivided into two
459 recording phases with a minimum 3-day rest period in between (“Phase 1”; Days 3-5 and
460 “Reversal Phase”; Days 6-8). On Day 1 (“habituation”), the mouse was connected to the optic
461 fiber cord and allowed to acclimatize. On Day 2 (“pre-test”), the mouse was placed in the 3-
462 compartment apparatus for 15 min to freely explore, while attached to the optic fiber cord but
463 without receiving any photostimulation; the preference for each compartment was evaluated.
464 On Days 3, 4 (“RT-PP”), entry into the assigned light-paired compartment (non-preferred in
465 pre-test) resulted in blue laser photostimulation delivered as continuous train of pulses (10ms

466 pulse width, 20Hz, 10mW). On Day 5 (“CR”), the time spent in each compartment was
467 measured for 15 min with no delivery of photostimulation. In the Reversal phase, the protocol
468 was repeated but with stimulation in the opposite compartment compared to Phase 1. “High-
469 power” experiments followed the same structure except that the mice received a stimulation
470 of higher power (5ms pulse width, 20Hz, 20mW).

471 For the Neutral Compartment Preference (NCP) test, a modified version of the test described
472 above was used with the following changes: Entry into either one of the two main
473 compartments was coupled to light-stimulation, while only entry the interconnecting
474 compartment had no consequence. The experiment took place on three consecutive days:
475 During the first two days (Stim1 & Stim2), the mice received stimulation upon entry in any of
476 the main compartments while the third day was stimulation-free and used to study the
477 presence of any conditioned responses (CR) induced by the experience with the stimulation.

478

479 **Experimental design and statistical analysis**

480 Regular and repeated measures (RM) two-way ANOVA and unpaired t-tests were used to
481 compare mean scores of Ctrl and cKO mice in behavioral tests. To analyze cocaine-induced
482 locomotion during CPP, a mixed-effects model was used. Post hoc comparisons were
483 performed by Sidak’s multiple comparison test. Unpaired t-test was used to compare mean
484 DA release between Chr2- and eYFP (control)-injected DAT-Cre, Calb2-Cre and NEX-Cre
485 mice for each region where the measurements were performed. Paired t-tests were used to
486 compare pre- and post- DNQX EPSP recordings. Two-way RM ANOVA with Day and
487 Chamber were used as factors throughout the optogenetic experiments followed by Tukey’s
488 post hoc test. When the days of stimulation were averaged, one-way ANOVA was used to
489 unravel the effect of compartment (paired, unpaired, neutral) on time spent and Tukey’s
490 multiple comparison test for post hoc analysis. Data are presented as mean \pm SEM unless

491 stated otherwise. Data analysis was performed with Prism8 (RRID: SCR_002798). Detailed
492 statistical information is shown in Table 1.

493

494 **Results**

495 *NeuroD6 mRNA is found in a modest population of the medial VTA where it co-localizes*
496 *extensively with dopaminergic markers and with a glutamatergic marker to minor degree*

497 To address the distribution pattern and neurotransmitter identity of *NeuroD6*-expressing
498 neurons, double-labeling fluorescent *in situ* hybridization was first performed in which
499 *NeuroD6* mRNA (Fig. 1A, C) was compared to Tyrosine hydroxylase (Th) mRNA encoding
500 the rate-limiting enzyme (TH) of DA synthesis (Fig. 1B, C). Using the distribution pattern of
501 Th mRNA as reference, DA neurons of the SNc and VTA were identified, including the
502 paranigral (PN), parainterfascicular (PIF), parabrachial pigmented nucleus (PBP),
503 interfascicular nucleus (IF) and rostral linear nucleus (RLi) subareas of the VTA (Fig. 1A- C).
504 *NeuroD6* mRNA was excluded from the SNc, but was detected in scattered VTA neurons.
505 Most *NeuroD6* neurons were found within the PN, PIF and PBP subareas of the VTA,
506 followed by fewer *NeuroD6* neurons in the IF and RLi (Fig. 1A, C). Co-detection analysis
507 showed that all neurons detected as positive for *NeuroD6* mRNA within the PN, PIF, PBP, IF
508 and RLi were positive for Th mRNA (Fig 1C). Quantification verified that 100% of *NeuroD6*
509 mRNA-positive cells in the PN/PIF, PBP, IF and RLi were positive for Th mRNA, while 12%
510 of all Th-expressing neurons within these VTA subareas contained *NeuroD6* mRNA (Fig.
511 1D). To further address the dopaminergic identity of *NeuroD6* neurons, co-detection of
512 *NeuroD6* mRNA with *Dat* mRNA, encoding the Dopamine transporter (DAT), was
513 performed. Similar to the overlap between *NeuroD6* and Th, all neurons detected as positive
514 for *NeuroD6* mRNA in the VTA were positive for *Dat* mRNA (Fig. 1E). To address the
515 neurotransmitter identity of the *NeuroD6*-mRNA-positive VTA neurons, co-detection

516 analyses of NeuroD6 mRNA with Vesicular glutamate transporter 2 (Vglut2) and Vesicular
517 inhibitory amino acid transporter (Vaat) mRNAs were performed for identification of
518 glutamatergic and GABAergic neurons, respectively. NeuroD6 mRNA showed some co-
519 localization with Vglut2 mRNA (Fig. 1F), while no or very few NeuroD6-positive cells in the
520 VTA were detected as positive for Vaaat mRNA (Fig. 1G). To address the overlap of
521 NeuroD6 mRNA with Vglut2 and Th mRNA in detail, triple-labeling *in situ* hybridization of
522 NeuroD6, Th and Vglut2 mRNAs was performed (Fig. 1H-P). This experiment confirmed
523 that all NeuroD6 VTA neurons within the PN, PIF, PBP, IF and RLi were detected as positive
524 for Th (Fig. 1H, K, N) and that some NeuroD6 neurons co-localized with Vglut2 (Fig. 1I,L,N).
525 Further, the experiment identified that these NeuroD6/Vglut2 double positive cells in the
526 VTA were positive for Th mRNA (Fig. 1J,M,N). Quantification verified that 100% of
527 NeuroD6 VTA neurons were positive for Th (NeuroD6+/Th+), and showed that 12% of these
528 NeuroD6+/Th+ VTA neurons were also positive for Vglut2 mRNA. 12% thus displayed a
529 NeuroD6+/Th+/Vglut2+ triple-positive molecular phenotype, while remaining 88% of
530 NeuroD6/Th neurons were negative for Vglut2 (NeuroD6+/Th+/Vglut2-) (Fig. 1O).
531 NeuroD6+/Th+/Vglut2+ and NeuroD6+/Th+/Vglut2- VTA neurons were distributed
532 throughout the VTA with highest density in PN, PIF and PBP subareas (Fig. 1M, P).

533 *Conditional ablation of the Vmat2 gene in NeuroD6-Cre VTA neurons – a model for spatially*
534 *restricted DA deficiency*

535 To analyze the consequences of lost ability for vesicular packaging of DA in NeuroD6 VTA
536 DA neurons, the *Slc18a2/Vmat2* gene encoding the Vesicular monoamine transporter 2
537 (VMAT2) was targeted using a NeuroD6-Cre (NEX-Cre) transgenic mouse line. By breeding
538 NEX-Cre mice with *Vmat2*^{lox/lox} mice, *Vmat2*^{lox/lox;NEX-Cre-1g} (cKO) and littermate control (Ctrl)
539 mice were produced (Fig. 2A). Upon PCR-based analysis of genotype, brains from Ctrl and
540 cKO mice were analyzed by *in situ* hybridization to verify loss of full-length Vmat2 mRNA

541 in cKO mice. Due to the scarcity of NeuroD6-positive neurons in the VTA, a Vmat2 mRNA
542 2-probe approach was utilized to allow detection of gene-targeted neurons. Vmat2 Probe 1
543 was designed to detect all cells positive for Vmat2 mRNA, while Vmat2 Probe 2 was
544 designed to bind mRNA derived from exon 2, the exon targeted for recombination by Cre
545 recombinase (Fig. 2B). In the ventral midbrain of control mice, Probe 1 (green) and Probe 2
546 (blue) were detected throughout the VTA and SNc areas with complete overlap (Fig. 2C, left
547 panel). In the corresponding area of cKO mice, the majority of cells were positive for both
548 Probe 1 and Probe 2 with complete overlap (Fig. 2C, right panel). However, throughout the
549 PN, PIF, PBP, IF VTA subareas, sparse cells showing green color only (Probe 1) were
550 detected, thus visualizing *Vmat2*-gene targeted cells among the mass of VTA DA neurons
551 positive for both Vmat2 Probe 1 and 2 (Fig. 2C, right panel). Having confirmed NEX-Cre-
552 mediated recombination of the floxed *Vmat2* gene within scattered neurons of the VTA, other
553 brain areas in which monoaminergic neurons reside were addressed by oligo *in situ*
554 hybridization. Apart from the modest VTA population positive for NeuroD6 mRNA,
555 NeuroD6 mRNA was not detected within any other monoaminergic cell group, identified by
556 Th and Vmat2 mRNA (Fig. 2-1). However, as previously reported (Goebbels et al., 2006),
557 NeuroD6 was abundant in several non-dopaminergic brain structures, primarily the cerebral
558 cortex and hippocampus (Fig. 2-1). In accordance with the lack of NeuroD6 in all
559 monoaminergic cell groups apart from the VTA, Vmat2 Probe 1 and Probe 2 showed
560 complete overlap in these areas, including locus coeruleus, ventromedial hypothalamus and
561 nucleus raphe obscurus, while none displayed labeling from Probe 1 only (Fig. 2D). These
562 experiments showed that in cKO mice, Vmat2 mRNA was selectively ablated within the
563 VTA. To address if the targeted deletion of *Vmat2* in NeuroD6 neurons of the VTA affected
564 the morphology of the midbrain DA system, distribution patterns of Th mRNA and TH

565 protein were addressed, none of which revealed any gross anatomical difference in the
566 dopaminergic system between Ctrl and cKO mice (Fig. 2E, Fig. 2-1).

567 *Heightened locomotor response to psychostimulants upon gene-targeting of Vmat2 in NEX-*
568 *Cre VTA neurons*

569 To address if it is possible to dissociate an explicit behavioral role of DA neurotransmission
570 exerted by NeuroD6 VTA DA neurons from the range of behaviors ascribed to the mDA
571 system, *Vmat2^{lox/lox;NEX-Cre-tg}* cKO mice were tested in a battery of tests relevant to the mDA
572 system and compared to *Vmat2^{lox/lox;NEX-Cre-wt}* Ctrl mice. To assess body weight, mice were
573 weighed every week from weaning to adulthood. cKO mice were similar to their Ctrl
574 littermates weight-wise (effect of age: $F_{(4,158)} = 79.8$, $p < 0.001$; genotype: $F_{(1,158)} = 4.67$ $p =$
575 0.032 ; no age x genotype interaction, no post hoc differences between genotypes) (Fig. 3A).

576 Baseline locomotion

577 The habituation response to a novel environment, a gross measure of stress and exploratory
578 behavior, was addressed. Both Ctrl and cKO mice showed the same rate of reaching a stable
579 plateau in baseline locomotion (effect of time: $F_{(5,160)} = 69.5$, $p < 0.001$; effect of genotype:
580 $F_{(1,32)} = 0.00912$, $p = 0.535$) (Fig. 3B).

581 Sucrose and ethanol preference

582 A sucrose bottle preference test was next performed. Both Ctrl and cKO mice preferred the
583 ascending concentrations of sucrose solutions over water (effect of concentration: $F_{(2,66)} =$
584 151 , $p < 0.001$), but no differences between the genotypes were observed (effect of genotype:
585 $F_{(1,33)} = 1.12$, $p = 0.297$) (Fig. 3C). The rewarding effect of alcohol was subsequently
586 measured by using increasing concentrations of ethanol (3, 6, 10%) presented in a bottle
587 preference test. Again, both Ctrl and cKO mice preferred the presented reward over water
588 (effect of concentration: $F_{(2,52)} = 14.2$, $p < 0.001$), but there was no difference between the
589 genotypes (effect of genotype: $F_{(1,26)} = 0.969$, $p = 0.334$). However, post hoc analysis showed

590 that Ctrl mice significantly preferred the 6% and 10% concentrations over the 3% solution
591 (§§§ $p < 0.001$ 3% vs 6% and 10% ethanol in ctrl mice), while a trend towards significant
592 differences in cKO mice was observed only between the 3% and 10% ethanol solutions (3%
593 vs 10%: $p < 0.072$) (Fig. 3D).

594 Cocaine- and amphetamine-induced locomotion

595 To address locomotor responses upon psychostimulant-injections, cocaine and amphetamine
596 administration protocols were applied and locomotion was measured. Upon administration of
597 acute ascending doses of cocaine (5, 10 and 20 mg/kg), both Ctrl and cKO mice displayed
598 increased locomotion in a dose-dependent manner, however, no significant differences were
599 observed between genotypes (effect of session: $F_{(3,99)} = 108$, $p < 0.001$; genotype, $F_{(1,33)} =$
600 1.65 , $p = 0.208$; session x genotype interaction: $F_{(3,99)} = 1$, $p = 0.396$) (Fig. 3E). Next, an
601 amphetamine sensitization protocol was applied. All mice responded to amphetamine with
602 hyperlocomotion, but the effect was significantly higher in cKO mice than control mice in
603 days 4, 5 and 17 of the experiment (effect of day: $F_{(5,160)} = 40.9$, $p < 0.001$; genotype, $F_{(1,32)} =$
604 9.09 , $p = 0.005$; day x genotype interaction: $F_{(5,160)} = 4.79$; $p < 0.001$; ctrl vs cKO Day 4 $p =$
605 0.011 , Day 5 $p < 0.001$, Day 17 $p = 0.029$) (Fig. 3F).

606

607 CPP

608 In order to study the reinforcing effects of psychostimulants, a CPP procedure was applied
609 (Fig. 3G). Both Ctrl and cKO mice showed preference to the cocaine- or amphetamine-paired
610 compartment over the saline-paired compartment with no significant difference between
611 genotypes (ctrl vs cKO cocaine: $p = 0.860$, amphetamine $p = 0.744$) (Fig. 3H,J). In addition to
612 preference, locomotion was monitored during the conditioning sessions. cKO mice displayed
613 increased locomotor responses after repeated administration of cocaine compared to Ctrl mice
614 (Fig. 3I, effect of session; $F_{(3,75)} = 4.4$, $p = 0.006$; effect of genotype $F_{(1,25)} = 5.2$, $p = 0.031$, no

615 differences in post hoc analysis). In contrast, in the CPP paradigm, repeated administration of
616 amphetamine did not induce elevated locomotion in cKO over Ctrl mice (Fig. 3K, effect of
617 session; $F_{(3,85)} = 24.0$, $p < 0.001$; effect of genotype $F_{(1,30)} = 0.0631$, $p = 0.803$).

618

619 *NeuroD6 mRNA co-localizes partly with Calb2 mRNA but Calb2 mRNA is abundant*
620 *throughout VTA and SNc*

621 To further characterize the molecular identity of NeuroD6 VTA neurons, *in situ* hybridization
622 was next used to address the putative overlap between NeuroD6 and Calb2 mRNAs.
623 Distribution patterns of NeuroD6 and Calb2 mRNAs within midbrain DA neurons were
624 recently described without addressing their putative overlap (Viereckel et al., 2016). In
625 contrast to the selective localization of NeuroD6 mRNA within the VTA and its exclusion
626 from the SNc, Calb2 mRNA was abundant in both VTA and SNc (Fig. 4A). The restricted
627 number of NeuroD6 neurons in the VTA showed partial overlap with Calb2 mRNA: 54% of
628 all NeuroD6 VTA neurons were positive for Calb2 mRNA while 20% of Calb2 neurons
629 expressed NeuroD6 mRNA (Fig. 4A). Further quantification within the VTA showed that
630 Calb2 mRNA was detected in 51% of all Th-neurons, with a similar match of Calb2/Dat co-
631 localization at 50% (Fig. 4B, C). Some Calb2 neurons in the VTA were positive for Vglut2
632 mRNA (7%)(Fig. 4D) while 20% of all Calb2 neurons in the VTA were positive for Viat
633 mRNA (Fig 4E).

634

635 *Spatially restricted striatal innervation by NeuroD6-Cre and Calb2-Cre VTA neurons*

636 Next, to allow analysis of projections, signaling properties and behavioral regulation of NEX-
637 Cre and Calb2-Cre VTA neurons, optogenetics was implemented. Upon infusion of viral
638 particles carrying a double-floxed *DIO-ChR2-eYFP* genetic construct encoding both
639 *Channelrhodopsin* (ChR2) and the *enhanced yellow fluorescent protein* (eYFP) into the VTA,

640 mice were analyzed in different parameters. DAT-Cre and Vglut2-Cre transgenic mice were
641 used as controls based on their representation of VTA and SNc dopaminergic and
642 glutamatergic neurons, respectively (Hnasko et al., 2012; Pascoli et al., 2015; Qi et al., 2016;
643 Stuber et al., 2010; Yoo et al., 2016). First, Cre-driven expression of the *DIO-ChR2-eYFP*
644 construct in DAT-Cre, Vglut2-Cre, Calb2-Cre and NEX-Cre mice was analyzed histologically
645 by comparing YFP with TH immunolabeling (Fig. 5A). In DAT-Cre, Vglut2-Cre, Calb2-Cre
646 and NEX-Cre mice, YFP fluorescent labeling was identified in the VTA, verifying the
647 activity of each Cre-driver to recombine the floxed optogenetic construct (Fig 5B, C, D, E, F).
648 YFP co-localized extensively with TH in the VTA. YFP was strongest and most abundant in
649 the VTA of DAT-Cre mice, while Vglut2-Cre, Calb2-Cre and NEX-Cre mice all showed
650 lower amount of cells positive for YFP (Fig 5B, C, D, E, F). Next, to reveal target areas,
651 sections throughout the entire brain of all four Cre-driver mouse lines were analyzed and
652 compared. Some target areas were the same for all four Cre-drivers, including the NAcSh and
653 ventral pallidum, while others differed, such as the distribution within the medial and lateral
654 habenula (Table 2). Overall, the density of YFP-positive fibers was substantially lower in
655 NEX-Cre and Calb2-Cre mice than in DAT-Cre and Vglut2-Cre mice. Following analysis of
656 sections throughout the brain, the VTA and striatum were analyzed in more detail. DAT-Cre
657 mice showed strong cellular YFP labeling within all VTA subareas (sparse in RLi) and within
658 the SNc, primarily on the injected side (Fig. 5C-C''). YFP-positive fibers were distributed
659 across the striatal complex including primarily the dorsomedial striatum, NAcSh, NAc core
660 and the olfactory tubercle (OT) (Fig. 5C-C''). Vglut2-Cre mice showed YFP-labeled cell
661 bodies primarily in the medial VTA with fibers innervating the NAc and OT (Fig 5D-D'').
662 Next, Calb2-Cre and NEX-Cre mice were addressed. Calb2-Cre mice showed similar
663 distribution of YFP-labeling as DAT-Cre within VTA, but the density was more sparse than
664 in DAT-Cre mice (Fig. 5E-E''). YFP-positive fibers in the striatal complex were detected in

665 the OT (Fig. 5E-E'). NEX-Cre mice showed a low number of YFP cells in the VTA (Fig. 5F-
666 F''), in accordance with the modest distribution of endogenous NeuroD6 mRNA described
667 above. Weak YFP fluorescence was detected in fibers throughout the NAcSh and OT (Fig.
668 5F-F''). The distribution pattern of YFP-positive cells in the VTA of NEX-Cre mice was
669 similar as distribution of endogenous NeuroD6 mRNA. However, the YFP appeared more
670 abundant than the above analyzed NeuroD6 mRNA. Quantification was performed to address
671 the overlap between YFP and TH. The majority of NEX-Cre/YFP and Calb2-Cre/YFP
672 neurons showed TH immunoreactivity, however, for both Cre-lines, a number of YFP cells
673 were negative for TH (NEX-Cre/ChR2: TH+: 4013 ± 21.72 , eYFP+ 965 ± 4.17 , double: 715
674 ± 3.24 ; Calb2-Cre/ChR2: TH+: 4187 ± 18.9 , eYFP+: 1396 ± 6.04 , double: 939 ± 4.69). In
675 total, 74% of NEX-Cre and 67% of Calb2-Cre neurons showed overlap between YFP and TH
676 (Fig. 5G,H).

677 *Optogenetic stimulation in striatal target areas of NeuroD6 and Calb2 VTA neurons verifies*
678 *DA release*

679 To address neurotransmitter release, extracellular DA concentration upon optogenetic
680 stimulation was recorded using fast-scan cyclic voltammetry in slice preparations. DAT-Cre,
681 NEX-Cre and Calb2-Cre mice injected with the same *DIO-ChR2-eYFP* construct as above
682 (Fig. 6A) were analyzed upon photostimulation and subsequent recording within the NAcSh
683 and OT (Fig. 6B). Cre-mice injected with *DIO-eYFP* were used as controls. DA levels (~1
684 μM) were readily recorded upon photostimulation in both the NAcSh of DIO-ChR2 injected
685 DAT-Cre ($0.9699 \pm 0.1471 \mu\text{M}$) and NEX-Cre mice ($0.4701 \pm 0.08043 \mu\text{M}$), while a lower
686 signal was obtained in the NAcSh of Calb2-Cre/ChR2 mice ($0.01509 \pm 0.002845 \mu\text{M}$) (Fig.
687 6C,D). Upon photostimulation and recording in the OT, lower DA levels (~200 nM) than
688 those measured in the NAcSh were obtained in DAT-Cre/ChR2 mice ($0.2129 \pm 0.01291 \mu\text{M}$)
689 while even smaller levels were detected in both Calb2-Cre/ChR2 ($0.02097 \pm 0.002712 \mu\text{M}$)

690 and NEX-Cre/ChR2 mice ($0.01362 \pm 0.002304 \mu\text{M}$) (Fig. 6C,D). Despite comparably low in
691 size, all DA levels recorded in mice expressing the ChR2-YFP were significantly larger than
692 in mice injected with the control virus (DAT-Cre, NAcSh ChR2: $0.9699 \pm 0.1471 \mu\text{M}$, eYFP:
693 $0.006802 \pm 0.0008813 \mu\text{M}$, $t_{(9)}=6.55$ $p < 0.0001$, OT ChR2 $0.2129 \pm 0.01291 \mu\text{M}$ vs eYFP
694 $0.004649 \pm 0.0009871 \mu\text{M}$, $t_{(9)}=16.08$ $p < 0.0001$; NEX-Cre, NAcSh ChR2: 0.4701 ± 0.08043
695 μM , eYFP: $0.0102 \pm 0.001682 \mu\text{M}$, $t_{(9)}=5.716$ $p < 0.0001$, OT ChR2: 0.01362 ± 0.002304
696 μM , eYFP: $0.005791 \pm 0.0008003 \mu\text{M}$, $t_{(9)}=3.209$ $p = 0.0049$; Calb2-Cre, NAcSh ChR2:
697 $0.01509 \pm 0.002845 \mu\text{M}$, eYFP: $0.006087 \pm 0.001746 \mu\text{M}$, $t_{(9)}=2.696$ $p = 0.0148$, OT ChR2:
698 $0.02097 \pm 0.002712 \mu\text{M}$, eYFP $0.007081 \pm 0.001315 \mu\text{M}$, $t_{(9)}=4.607$ $p = 0.0002$) (Fig. 6C,D).
699

700 *Optogenetic stimulation in striatal target areas of NeuroD6 and Calb2 VTA neurons reveals a*
701 *glutamatergic post-synaptic response*

702 To address the presence of post-synaptic currents in NAcSh and OT neurons upon
703 optogenetic activation, patch clamp electrophysiology was implemented in NEX-Cre and
704 Calb2-Cre injected with *DIO-ChR2-eYFP* (Fig. 7). Upon optogenetic stimulation, 82% of
705 neurons in the NAcSh NEX-Cre mice (18 out of 22 cells) and 87% of OT neurons in Calb2-
706 Cre mice (13 out of 15 cells) showed excitatory post-synaptic currents (EPSCs, NEX-Cre
707 NAcSh, mean amplitude 28 ± 6.8 pA; Calb2-Cre OT, mean amplitude 39 ± 7.7 pA;) (Fig.
708 7B,C). In both cases, EPSCs were almost completely abolished after bath application of 10
709 μM of the AMPA receptor antagonist DNQX, demonstrating that the recorded currents are
710 AMPA receptor-mediated (NEX-Cre NAcSh mean amplitude: control: 33 ± 13 pA, DNQX
711 1.5 ± 0.96 pA $t_{(5)}=2.602$ $p = 0.0481$; Calb2-Cre OT, mean amplitude: control: 46 ± 16 pA,
712 DNQX: 0.74 ± 0.74 pA $t_{(4)}=2.867$ $p = 0.0456$) (Fig. 7D). The synaptic delay of the EPSCs
713 was short (NEX-Cre NAcSh 3.3 ± 0.25 ms; Calb2-Cre OT 3.6 ± 0.21 ms). In contrast, the

714 mean decay time was longer in the OT than in NAcSh (NEX-Cre NAcSh 5.3 ± 0.5 ms; Calb2-
715 Cre OT 7.8 ± 0.62 ms). No inhibitory/GABA-receptor mediated currents were observed
716 during recordings in either NEX-Cre or Calb2-Cre mice (Fig. 7B).

717

718 *Optogenetic activation of NeuroD6 VTA neurons, but not Calb2 VTA neurons, induces place*
719 *preference*

720 Finally, *in vivo* optogenetic stimulation in the VTA of NEX-Cre and Calb2-Cre mice was
721 applied to assess if this would induce place preference behavior. Again, DAT-Cre and
722 Vglut2-Cre mice were used as references for comparison to Calb2-Cre and NEX-Cre mice.
723 Mice received *DIO-ChR2-eYFP* or *DIO-eYFP* (control) injection and implantation of optic
724 fibers above the VTA (Fig. 8A,G), and were analyzed for real-time place preference (RT-PP)
725 and conditioned response (CR) (Fig. 8A).

726

727 Analysis of RT-PP and CR in DAT-Cre and Vglut2-Cre mice

728 DAT-Cre mice displayed a significant preference to the light-paired compartment on every
729 day of stimulation (Fig. 8B left, effect of compartment $F_{(2,18)} = 51.8$, $p < 0.001$; day x
730 compartment interaction $F_{(12,108)} = 33$, $p < 0.001$, *** $p < 0.001$ paired vs unpaired
731 compartment). This place preference was also evident when the effect of stimulation was
732 averaged for the four experimental days (Fig. 8B, right, effect of compartment $F_{(2,6)} = 166$, $p <$
733 0.001 *** $p < 0.001$ vs paired compartment). In the absence of stimulation, on days 5 and 8,
734 DAT-Cre mice demonstrated a conditioned response for the previous light-paired
735 compartment (Fig. 8B, *** $p < 0.001$ paired vs unpaired). Control mice (DAT-Cre negative or
736 DAT-Cre injected with *DIO-eYFP*) did not display any preference towards the stimulation
737 (Fig. 8-1A, left effect of compartment $F_{(2,4)} = 4.26$, $p = 0.102$; day x compartment interaction,
738 $F_{(12,24)} = 0.898$ $p = 0.562$, * $p < 0.05$ paired vs unpaired compartment; right: effect of

739 compartment $F_{(2,6)} = 48.7$ $p < 0.001$, $***p < 0.001$ $###p < 0.001$ neutral vs paired and
740 unpaired respectively; Fig. 8-1B, left effect of compartment $F_{(2,4)} = 27.9$, $p = 0.004$, day x
741 compartment interaction $F_{(12,24)} = 0.767$ $p = 0.677$, $***p < 0.001$ paired vs unpaired
742 compartment; right: effect of compartment $F_{(2,6)} = 2.97$, $p = 0.127$; Fig. 8-1C, left: effect of
743 compartment $F_{(2,10)} = 18.6$, $p < 0.001$, day x compartment interaction $F_{(12,60)} = 0.963$, $p =$
744 0.494 , right: effect of compartment $F_{(2,6)} = 9.27$, $p = 0.015$, $*p < 0.05$ $\#p < 0.05$ neutral vs
745 paired and unpaired respectively). These results were in accordance with the literature (Yoo et
746 al., 2016) and thereby validated the experimental setup. In contrast to the strong place
747 preference induced by stimulation in DAT-Cre mice, Vglut2-Cre mice analyzed in the same
748 setup displayed a preference for the unpaired compartment (Fig. 8C, left: effect of
749 compartment $F_{(2,12)} = 40.9$, $p < 0.001$ and day x compartment interaction $F_{(12,72)} = 16.1$, $p <$
750 0.001 , $***p < 0.001$ paired vs unpaired; right: effect of compartment $F_{(2,6)} = 162$, $p < 0.001$,
751 $***p < 0.001$ vs paired, $###p < 0.001$ vs unpaired). To further verify this observation, the
752 protocol was modified so that the mice would receive photostimulation upon entry to either
753 one of the main compartments but not upon entry into the interconnecting neutral
754 compartment (“Neutral Compartment Preference”, Fig. 8-1Ii). Once again, Vglut2-Cre mice
755 preferred to spend time in the area lacking stimulation (Fig. 8-1Iii, effect of compartment $F_{(2,8)}$
756 $= 70.9$, $p < 0.001$ and day x compartment interaction $F_{(4,16)} = 6.90$ $p = 0.002$, $**p < 0.01$, $***p$
757 < 0.001 neutral vs paired compartments, Fig. 8-1Iiii effect of compartment $F_{(2,2)} = 54.2$, $p =$
758 0.018 , $*p < 0.05$ neutral vs paired compartments). In the current setups, optogenetic VTA-
759 stimulation of DAT-Cre mice thus leads to place preference while same stimulation of
760 Vglut2-Cre mice causes an avoidance to any compartment that activates photostimulation.

761

762 Analysis of RT-PP and CR in Calb2-Cre and NEX-Cre mice

763 Using these behaviors as references and for comparison in the place preference setup, Calb2-
764 Cre mice showed a strikingly different behavior: Neither preference nor avoidance was
765 detected but instead, mice spent equal amount of time in both main compartments (Fig. 8D,
766 left, effect of compartment $F_{(2,12)} = 27$, $p < 0.001$, day x compartment interaction, $F_{(12,72)} =$
767 1.45, $p = 0.163$ and no differences between paired vs unpaired across days; right: effect of
768 compartment $F_{(2,6)} = 90.1$, $p < 0.001$, no differences between paired vs unpaired, $***p <$
769 0.001 , $###p < 0.001$ neutral vs paired and unpaired, respectively). When analyzing if
770 optogenetic activation of NEX-Cre VTA neurons would cause place preference, a significant
771 behavioral response towards the photostimulation was observed (Fig. 8E left: effect of
772 compartment $F_{(2,8)} = 76.8$, $p < 0.001$, day x compartment interaction, $F_{(12,48)} = 4.63$, $p <$
773 0.001). NEX-Cre mice responded weakly to VTA-photostimulation on Days 3 and 4, but on
774 Days 6 and 7, NEX-Cre mice preferred the light-paired compartment ($*p = 0.02$, $***p <$
775 0.001 paired vs unpaired). However, no CR was observed on either Day 5 or 8 (Fig.8E left).
776 By averaging the results of all four RT-PP days, NEX-Cre mice showed a significant
777 preference for paired over unpaired and neutral compartments (Fig. 8E right, effect of
778 compartment $F_{(2,6)} = 39.7$, $p < 0.001$ $*p = 0.013$ $***p < 0.001$ vs paired, $##p = 0.008$ neutral
779 vs unpaired).

780

781 Analysis of RT-PP and CR in DAT-Cre, Calb2-Cre and NEX-Cre mice using higher power
782 stimulation

783 While the result above demonstrated that activation of NEX-Cre VTA neurons induced place
784 preference behavior, higher power stimulation (5 ms pulse width, 20 Hz, 20 mW) was
785 subsequently used to test if these laser parameters would boost the observed behavioral
786 response. Again, DAT-Cre mice showed a strong preference for the light-paired chamber
787 (Fig. 8-1E left, effect of compartment $F_{(2,6)} = 105$, $p < 0.001$, day x compartment interaction

788 $F_{(12,36)} = 22.6, p < 0.001, ***p < 0.001$ paired vs unpaired; right, effect of compartment $F_{(2,6)}$
789 $= 404, p < 0.001, ***p < 0.001$ unpaired and neutral vs paired) while Calb2-Cre mice
790 continued not to respond to the VTA photostimulation (*Fig. 8-1F*, left: effect of compartment
791 $F_{(2,12)} = 12.5, p = 0.001$, day x compartment interaction $F_{(12,72)} = 0.469, p = 0.927$; right:
792 effect of compartment $F_{(2,6)} = 47.3, p < 0.001, ***p < 0.001$ & $###p < 0.001$ neutral vs
793 unpaired and paired). In contrast, NEX-Cre mice showed a significant preference also with
794 this higher power stimulation (*Fig. 8-1G* left, effect of compartment $F_{(2,6)} = 48.3, p < 0.001$,
795 day x compartment interaction $F_{(12,36)} = 8.58, p < 0.001, **p = 0.003, ***p < 0.001$ paired vs
796 unpaired; right, effect of compartment $F_{(2,6)} = 178, p < 0.001, ***p < 0.001$ paired vs unpaired
797 and neutral. $###p < 0.001$ unpaired vs neutral). Finally, to further validate the role of NEX-
798 Cre VTA neurons in place preference, a subset of NEX-Cre mice was bilaterally injected with
799 *DIO-ChR2-eYFP* and tested in the same protocol under normal and high-power light
800 stimulation (*Fig. 8-1H* and *Fig. 8F*). Mice preferred the light-paired side over the unpaired
801 under both conditions, and high-power stimulation accentuated the preference towards the
802 light paired compartment which reached a 3-fold increase compared to the unpaired (standard
803 power: *Fig. 8-1H*, left, effect of compartment $F_{(2,6)} = 43.3, p < 0.001$, day x compartment
804 interaction $F_{(12,36)} = 2.13, p = 0.04$; right, effect of compartment $F_{(2,6)} = 331, p < 0.001, ***p <$
805 0.001 vs paired $###p < 0.001$ vs unpaired. High power: *Fig. 8F*, left, effect of compartment
806 $F_{(2,6)} = 36.5, p < 0.001$, day x compartment interaction $F_{(12,36)} = 9.03, p < 0.001, ***p < 0.001$
807 paired vs unpaired; right, effect of compartment $F_{(2,6)} = 106, p < 0.001, ***p < 0.001$ paired vs
808 unpaired and neutral, $#p = 0.011$ unpaired vs neutral). However, unlike DAT-Cre mice, NEX-
809 Cre mice did not show any CR in any RT-PP experiment (*Fig. 8E* day 5 paired vs unpaired
810 $p > 0.999$, day 8 paired vs unpaired $p = 0.937$; *Fig. 8F* day 5 paired vs unpaired $p > 0.999$, day
811 8 paired vs unpaired $p = 0.989$).

812

813 **Discussion**

814 It is well established that the VTA is involved in a range of functions, including behavioral
815 reinforcement, reward, aversion, motivation and incentive salience (Morales and Margolis,
816 2017). However, an area of active investigation is how the VTA can possess the ability to
817 contribute to all of these diverse functions, some even contrasting. It is now becoming
818 increasingly clear that functional diversity within the mDA system might be matched by
819 molecular and anatomical heterogeneity (Lammel et al., 2011, 2012; Morales and Margolis,
820 2017; Poulin et al., 2018; Roeper, 2013). Why is this important? The possibility to determine
821 the exact identity of neurons that contribute to a particular behavior opens up entirely new
822 perspectives in the opportunity to selectively target only those neurons that contribute to
823 clinical symptoms without side-effects caused by affecting adjacent neuronal population. In
824 this study, we used Cre-driven mouse genetics and optogenetics to begin to disentangle the
825 contribution of the newly described NeuroD6 VTA subtype (Khan et al., 2017; Kramer et al.,
826 2018; Viereckel et al., 2016) in reward-related behaviors commonly ascribed to the VTA DA
827 system. The main finding of our studies is that despite their restricted number, NeuroD6 VTA
828 neurons contribute to psychostimulant-induced hyperlocomotion and that their activation
829 induces place preference behavior.

830 *NeuroD6 VTA neurons represent a modest neuronal population within the VTA with*
831 *molecular capacity for dopaminergic and glutamatergic neurotransmission*

832 In the current study, we showed that NeuroD6 VTA neurons constitute a modest proportion
833 (circa 12%) of all VTA neurons expressing the gene encoding TH within the PN, PIF, PBP,
834 IF and RLi subareas. Within these VTA subareas, all NeuroD6-positive neurons were positive
835 for both Th and Dat mRNAs, markers of dopaminergic neurons. In addition, while no or very
836 few NeuroD6 neurons were positive for Viaat mRNA, a marker of GABAergic neurons, 12%

837 of the NeuroD6/Th double-positive neurons within the VTA were positive for Vglut2 mRNA,
838 suggesting a capacity for dual dopaminergic/glutamatergic neurotransmission. Indeed,
839 DA/glutamate co-release has in several studies been shown as a property of certain mDA
840 neurons where it has been proposed to play a role in reward-related behavior reinforced by
841 DA (recently reviewed in Trudeau and El Mestikawy, 2018). The identification of co-labeling
842 of NeuroD6 mRNA with Th, Dat and Vglut2 mRNAs within distinct neurons was partly in
843 accordance with our analysis of a NEX-Cre transgenic mouse line, implemented here to
844 achieve manipulation of the NeuroD6 VTA neurons, which identified substantial co-
845 localization between NEX-Cre-driven reporter gene expression (YFP) and TH
846 immunofluorescence. However, lack of TH/YFP co-localization was also identified. The
847 findings showing that the majority of NeuroD6 VTA neurons expressed DA markers fitted
848 with our electrophysiological data in which optogenetic VTA stimulation of NEX-Cre
849 neurons enabled the identification of DA release, as further discussed below. Further,
850 optogenetic stimulation also gave rise to EPSCs of glutamatergic nature, while no
851 GABAergic currents were detected, in agreement with the co-localization of NeuroD6 mRNA
852 with Vglut2 mRNA but lack of significant co-localization with Viaat mRNA.

853

854 In the context of transgenic mice, it is noteworthy that our result showing non-complete
855 overlap between NEX-Cre-driven reporter gene expression and TH, which contrasts the
856 parallel finding that all VTA neurons positive for endogenous NeuroD6 mRNA also label for
857 Th mRNA, are in accordance with a recent study in which a substantial number of non-
858 dopaminergic NEX-Cre VTA neurons were identified (Kramer et al., 2018). Collectively,
859 these findings propose that interpretation of VTA-data originating from the current NEX-Cre
860 mouse line should be considered with awareness of complex downstream neurocircuitry.
861 Further, as extensively discussed in the literature, regulatory promoters implemented

862 experimentally to drive Cre expression may give rise to transient and/or ectopic Cre activity
863 that fails to mimic endogenous gene expression due to gene regulatory events, not least during
864 developmental phases. Indeed, patterns of ectopic Cre activity have been described for other
865 transgenic mouse lines, including DAT-Cre and TH-Cre transgenic mouse lines commonly
866 implemented for the study of DA neurons (Lammel et al., 2015; Lindeberg et al., 2004;
867 Morales and Margolis, 2017; Nordenankar et al., 2015; Pupe and Wallén-Mackenzie, 2015;
868 Stamatakis et al., 2013; Stuber et al., 2015). While the current NEX-Cre transgenic line has
869 been thoroughly validated recently for the study of VTA neurons (Khan et al., 2017; Kramer
870 et al., 2018), to direct selectivity to VTA DA neurons, we here implemented a conditional
871 genetic approach to specifically abrogate vesicular packaging of DA in NEX-Cre neurons,
872 while we used optogenetically-driven neuronal activation to study effects upon direct
873 stimulation of NEX-Cre VTA neurons.

874

875 *Targeting of the Vmat2 gene in NEX-Cre VTA DA neurons allowed identification of a role in*
876 *psychostimulant-mediated response*

877 To enable the study of how reward-related behaviors classically associated with the mDA
878 system would be affected if the NEX-Cre DA neuron subtype lost its ability for dopaminergic
879 function, a conditional gene-targeting approach was implemented in which VMAT2 was
880 ablated specifically from NEX-Cre neurons. Since we could show that NeuroD6 and Vmat2
881 mRNAs only co-localized within the VTA, no other monoaminergic population should suffer
882 from loss of VMAT2 by this approach. Indeed, the results confirmed that Vmat2 mRNA was
883 selectively knocked out within the VTA, while all other monoaminergic neurons maintained
884 normal Vmat2 mRNA. Thus, the *Vmat2^{lox/lox;NEX-Cre}* mouse line forms a new mouse model of
885 DA-release deficiency from a restricted group of VTA DA neurons characterized by NeuroD6
886 promoter activity. Based on the importance of mDA system in processing natural and drug

887 rewards (Baik, 2013; Di Chiara and Bassareo, 2007; Ikemoto, 2007; Kalivas et al., 1992;
888 Robinson and Berridge, 1993), we addressed the behavioral responses of *Vmat2*^{lox/lox;NEX-Cre-tg}
889 cKO mice and *Vmat2*^{lox/lox;NEX-Cre-wt} control mice to sugar, ethanol and the psychostimulants
890 amphetamine and cocaine. cKO mice displayed higher locomotor activation upon repeated
891 administration of psychostimulants than control mice. In contrast, sugar preference and
892 conditioned place preference to cocaine and amphetamine were similar between cKO and
893 control mice, and both genotype groups showed a preference for increasing dose of ethanol,
894 albeit in different patterns.

895 While acute administration of cocaine failed to cause differences in locomotor responses
896 between cKO and control mice, repeated administration caused exaggerated locomotor
897 behavior in cKO mice when measured in the CPP paradigm. In contrast, with repeated
898 amphetamine injections, the locomotor response was elevated above control levels in the open
899 field, but not in the CPP. The tests implemented were designed to study different behavioral
900 parameters, and results obtained in different setups and by different drugs are therefore not
901 directly comparable. What may seem as apparent discrepancies might be related to several
902 different properties. Firstly, the size and properties of the test environment were substantially
903 different between setups. The open field test took place in an environment that resembled the
904 home-cage. Locomotion was recorded during the conditioning phase when the mice were
905 confined to a much smaller compartment with specific patterns and no bedding. Secondly, the
906 injection regime differed between tests. In the open field, mice received acute injections of
907 cocaine or were sensitized to amphetamine by receiving daily injections after a 30-min
908 habituation period. In contrast, in the CPP experiment, the mice received in total four
909 injections of the drug in two non-consecutive days without any previous habituation period.
910 Finally, the recording period was shorter in the CPP compared to the open field (30 min vs
911 1.5 h), a parameter that could mask the long-lasting effects of amphetamine on locomotion.

912 Further, the observation of heightened, rather than reduced, psychostimulant-induced
913 locomotion might seem counter-intuitive: Loss of VMAT2 should lead to decreased
914 packaging and release of DA which might be expected to cause reduced locomotion
915 compared to control levels. However, the results obtained from our spatially selective cKO
916 mice are similar to the heightened amphetamine-induced hyperlocomotion observed in a
917 study of mice heterozygous for *Vmat2* in all DAT-Cre neurons (Isingrini et al., 2016). Thus,
918 lowering the level of VMAT2 throughout all DAT-Cre neurons or ablating it within the NEX-
919 Cre VTA DA population give rise to similar behavioral consequences. Further analyses
920 focused around VMAT2 in psychomotor behavior will be necessary to pin-point this matter,
921 however, developmental adaptations, a common feature of KO strategies induced during
922 embryonal development, may underlie the heightened locomotor response.

923 *Optogenetic stimulation of the VTA in NEX-Cre mice induces DA release and glutamatergic*
924 *EPSCs*

925 Complementary to the cKO approach, we used optogenetics-based experiments in which the
926 NEX-Cre VTA population could be directly stimulated. This type of manipulation provides
927 high spatial and temporal resolution (Deisseroth, 2015) and thus has the advantage of
928 enabling selective stimulation of Cre-driven neurons in real time with the benefit of directly
929 pin-pointing the role of molecularly defined neurons in measurable behavior. By analysis of
930 optogenetic reporter gene (eYFP) expression upon injection into the VTA of NEX-Cre mice,
931 we showed that NeuroD6 VTA neurons projected mainly to the NAcSh of the striatal
932 complex, with substantially lower density than observed upon similar injection in DAT-Cre
933 and *Vglut2*-Cre mice used here as controls (Hnasko et al., 2012; Pascoli et al., 2015; Qi et al.,
934 2016; Stuber et al., 2010; Yoo et al., 2016). NEX-Cre VTA projections also reached several
935 additional areas, but with even lower density than seen in the NAcSh, including the OT,

936 medial habenula and ventral pallidum. In accordance with the co-localization of eYFP with
937 TH immunoreactivity, we could verify that NEX-Cre VTA neurons released DA in both the
938 NAcSh and OT upon optogenetic stimulation in the VTA. Although the levels were lower
939 than those observed upon similar stimulation of DAT-Cre-positive VTA neurons, they were
940 significantly higher than those observed in control experiments, demonstrating that the NEX-
941 Cre VTA population indeed releases measurable amounts of DA in their target areas. To
942 investigate whether the TH-negative cellular population, present most profoundly in the
943 medial VTA, was of glutamatergic or GABAergic nature, patch-clamp electrophysiology was
944 performed which showed that optogenetic stimulation of NEX-Cre terminals induced EPSCs,
945 but not IPSCs, in NAcSh, thus verifying glutamatergic neurotransmission. While
946 glutamatergic post-synaptic currents were evidently a result of the optogenetic stimulation of
947 NEX-Cre VTA neurons, it remains to be established if the rare endogenous NeuroD6/Vglut2
948 double-positive neurons observed in our histological analysis are sufficiently potent to drive a
949 similar post-synaptic response in the natural situation, that is, upon excitation of the NeuroD6
950 VTA neurons in a non-transgenic context. Finally, the current setup did not allow us to
951 conclude if the EPSCs were of mono-or polysynaptic nature. The short onset of EPSCs was
952 suggestive of monosynaptic transmission, however, electrophysiological approaches
953 combined with pharmacological agents will be necessary to fully define the signaling
954 properties.

955 *Optogenetic stimulation of NEX-Cre VTA neurons reveals a role in place preference behavior*

956 Optogenetic stimulation of the mDA system of TH-Cre and DAT-Cre mice has been
957 demonstrated to potently induce DA release and real time place preference (Stuber et al.,
958 2010; Tsai et al., 2009; Yoo et al., 2016). The same type of activation of VTA in Vglut2-Cre
959 mice has been described to cause post-synaptic glutamatergic currents and to induce either

960 place preference or place avoidance, depending on stimulation parameters (Hnasko et al.,
961 2012; Qi et al., 2016; Wang et al., 2015; Yoo et al., 2016). Using DAT-Cre and Vglut2-Cre
962 mice as references, we could show here that optogenetic stimulation within the VTA of NEX-
963 Cre mice induced a significant preference for the light-paired compartment. The magnitude of
964 the preference observed was, however, smaller in NEX-Cre than in DAT-Cre mice. This
965 difference is likely related to the substantially smaller population of VTA neurons activated
966 upon photostimulation in the NEX-Cre compared to DAT-Cre VTA and the different
967 projection patterns of these neuronal populations: VTA-injection of ChR2-YFP in DAT-Cre
968 mice results in strong YFP-fluorescence in all innervation areas ascribed to the mDA system.
969 In contrast, the same injection into the VTA of NEX-Cre mice results in substantially lower
970 YFP-derived fluorescence in the VTA and sparse fluorescence in target areas.

971 Despite smaller magnitude, the ability of NEX-Cre VTA neurons to induce real time place
972 preference is an important finding as it demonstrates the possibility of identifying spatially
973 restricted groups of VTA neurons that are sufficient to induce a measurable behavior. Further
974 arguing for the importance of this result, the optogenetically induced preference behavior
975 displayed by NEX-Cre mice was strengthened by viral injections in bilateral, rather than
976 unilateral, manner as well as by increased laser power. The results of these experimental
977 manipulations suggest that the enhanced recruitment of NEX-Cre neurons strengthened the
978 behavioral output. While additional studies will be required to completely disentangle the
979 behavioral role of NeuroD6 VTA neurons, the current optogenetics-based setup already
980 enabled us to demonstrate that VTA activation in NEX-Cre mice could induce place
981 preference in real-time, but that it failed to result in conditioned response, defined as
982 significant place preference even in absence of actual optogenetic stimulation. This contrasts
983 the strong conditioned response observed in the DAT-Cre mice, and hence, activation of VTA
984 populations in NEX-Cre mice and DAT-Cre mice differ in more than one parameter:

985 Magnitude in real time place preference and presence of a detectable conditioned response. In
986 contrast to the preference behavior displayed by NEX-Cre and DAT-Cre mice, optogenetic
987 stimulation of VTA Vglut2-Cre neurons led to real time place avoidance defined here as
988 reduced time spent in the stimulation-paired compartment. This result is consistent with a
989 recent study which found that real time avoidance coincided with a frequency-dependent
990 increase in entries to the light-paired compartment and robust self-stimulation in an operant
991 task (Yoo et al., 2016). In contrast, another study found that photostimulation of Vglut2-Cre
992 neurons in VTA induced modest real time place preference and self-stimulation (Wang et al.,
993 2015). These data show that the behavioral effects of VTA glutamate neuron stimulation are
994 sensitive to the task, including the design of the apparatus and stimulus parameters. In this
995 context, it is noteworthy that VTA neurons of the NEX-Cre transgenic mouse line, with their
996 mixture of dopaminergic and glutamatergic signaling properties, might have shown lower
997 level of place preference than DAT-Cre mice not only due to the smaller number of neurons
998 and more sparse projections, but also as their activation might have caused a glutamate-
999 mediated avoidance behavior that counterbalanced the behavioral preference for light-
1000 stimulation.

1001

1002 *NeuroD6 and Calb2 mRNAs show partial overlap but NEX-Cre and Calb2-Cre VTA neurons*
1003 *have distinct projections and role in behavior*

1004 Parallel to the focus on NeuroD6 VTA neurons in neurocircuitry and behavioral regulation,
1005 our histological analysis enabled us to identify a degree of co-localization between NeuroD6
1006 and Calb2 mRNAs. While NeuroD6 mRNA was uniquely found in the VTA and excluded
1007 from the SNc, Calb2 mRNA was found distributed throughout these dopaminergic areas.
1008 However, histological analysis showed a degree of co-localization between NeuroD6 and
1009 Calb2 mRNAs, a finding which adds to the recent molecular description of NeuroD6 as co-

1010 localized with gastrin-releasing peptide (GRP) and additional markers (Khan et al., 2017;
1011 Kramer et al., 2018; Poulin et al., 2018). Beyond the partial co-localization of NeuroD6 and
1012 Calb2 mRNAs, the results show that Calb2 VTA neurons constitute a substantially larger
1013 proportion within the mDA population, show considerable expression of the gene encoding
1014 VIAAT, and are present in the SNc, an area devoid of NeuroD6 neurons. Our
1015 neurophysiological circuitry analyses of Calb2-Cre mice showed that Calb2-Cre VTA
1016 neurons belong to the category of VTA/SNc neurons that projects to the OT where their
1017 stimulation resulted in DA release and glutamatergic post-synaptic currents. While it was
1018 recently described that activation of dopaminergic fibers from VTA to the medial OT can
1019 induce place preference in DAT-Cre mice (Zhang et al., 2017), a similar response was not
1020 observed here upon Calb2-Cre VTA stimulation. These differences might be explained by the
1021 difference in density of the innervation patterns in the OT between the DAT-Cre and Calb2-
1022 Cre mice. The difference in preference behavior between NeuroD6-Cre and Calb2-Cre mice
1023 shows that distinct VTA neurocircuitry is crucial for the behavioral output.

1024 *Unraveling the behavioral roles of NeuroD6 VTA neurons stands to benefit current decoding*
1025 *of VTA-related disorders*

1026 The behavioral complexity mediated by the VTA is implicated in a range of neuropsychiatric
1027 conditions including substance use disorder, schizophrenia and ADHD for which clinical
1028 interventions based on increasing, decreasing, stabilizing or modulating the mDA system are
1029 commonly prescribed. In addition, since VTA DA neurons are less susceptible to
1030 degeneration in PD than SNc DA neurons, molecular differences are intensively searched for.
1031 GRP, in several studies identified as a marker for VTA DA neurons (Chung et al., 2005;
1032 Greene et al., 2005; La Manno et al., 2016; Viereckel et al., 2016) was recently shown to co-
1033 localize with NeuroD6 (Kramer et al., 2018). Several lines of evidence suggest that a discrete

1034 NeuroD6/GRP VTA subtype should be of specific interest: Overexpression of the gene
1035 encoding GRP increased the survival rate of cultured DA neurons in a parkinsonian
1036 experimental model (Chung et al., 2005) and GRP-positive mDA neurons remain in biopsies
1037 from deceased PD patients (Viereckel et al., 2016). Further, NeuroD6 increases neuronal
1038 survival in a toxin model of PD (Kramer et al., 2018). The NeuroD6/GRP VTA subtype might
1039 thereby possess resistance to PD. Our current results show that, despite their modest
1040 representation within the VTA, NeuroD6-expressing VTA neurons are implicated in distinct
1041 aspects of reward-related behavior. Their resistance to PD may thus contribute to the cause of
1042 behavioral dysfunction observed in the non-motor symptom domain of PD, including
1043 treatment-induced complications that resemble aspects of neuropsychiatric diseases, such as
1044 behavioral addictions (Cenci et al., 2015).

1045 Current molecular profiling of DA neuron subtypes should prove valuable for prospects of
1046 selective treatment in conditions related to VTA dysfunction. Of essence to achieve such
1047 selectivity is the systematic decoding of the explicit behavioral roles mediated by distinct
1048 VTA neurons. In this study, we initiated such analysis and now propose that NeuroD6 VTA
1049 neurons are of particular interest for further analysis of motivated and addictive behavior as
1050 they are here implicated in reward-related behavior measured as real time place preference
1051 and as their controlled dysregulation alters the responsiveness to psychostimulants. Our
1052 findings should prove useful for future investigations aimed at advancing the knowledge of
1053 VTA neurocircuitry in healthy conditions and in neuropsychiatric illness implicating the
1054 VTA.

1055 **Figure Legends**

1056 **Figure 1. NeuroD6 mRNA is found in a modest population of the VTA, co-localizes with**
1057 **dopaminergic markers and partially with a glutamatergic marker**

1058 (A-G) Double-fluorescent *in situ* hybridization (FISH) in the ventral midbrain of adult wild-
1059 type mice detecting the following mRNAs: **A, A'** NeuroD6 (red); **B, B'** Th (green); **C, C'**
1060 NeuroD6 (red) and Th (green). Th/NeuroD6 mRNA overlap shown in yellow. Low
1061 magnification to the left; close-ups to the right. Schematic outline shows borders for SNc and
1062 subregions of VTA: PN, PIF, PBP, IF, RLi. **D**, Quantification of percentage of NeuroD6-
1063 positive cells among all Th VTA cells; all NeuroD6 cells are positive for Th mRNA. **E**,
1064 NeuroD6 (red) and Dat (green), inset with high-magnification of Dat/NeuroD6 mRNA
1065 overlap (yellow); **F**, NeuroD6 (red) and Vglut2 (green); **G**, NeuroD6 (red) and Viaat (green),
1066 inset with high-magnification of Viaat-negative/NeuroD6-positive (red). (**H-P**) Triple-
1067 labeling FISH in the ventral midbrain of adult wild-type mice detecting: **H**, Th (blue); **I**,
1068 NeuroD6 (red); **J**, Vglut2 (green) mRNAs and their co-localization: **K**, NeuroD6/Th; **L**,
1069 NeuroD6/Vglut2; **M**, Th/NeuroD6/Vglut2. Cellular closeups: **N**, NeuroD6/Th (top),
1070 NeuroD6/Vglut2 (middle), Th/NeuroD6/Vglut2 (bottom). Arrows point to NeuroD6 mRNA-
1071 positive cells. **O**, Quantification of percentage of NeuroD6+/Th+/Vglut2+ and
1072 NeuroD6+/Th+/Vglut2+ neurons of the VTA; **P**, Schematic illustration of distribution pattern
1073 of NeuroD6+/Th+/Vglut2+ and NeuroD6+/Th+/Vglut2- neurons within the VTA (same as
1074 shown with experimental data in **M**). NeuroD6+/Th+/Vglut2- cells in magenta;
1075 NeuroD6+/Th+/Vglut2+ cells in cyan.

1076 Abbreviations: VTA, ventral tegmental area; SNc, substantia nigra *pars compacta*; PBP,
1077 parabrachial pigmented nucleus; PN, paranigral nucleus; PIF, parainterfascicular nucleus;
1078 RLi, rostral linear nucleus; IF, interfascicular nucleus.

1079

1080 **Figure 2. Conditional ablation of the *Vmat2* gene in NEX-Cre neurons – a model for**
1081 **spatially restricted DA deficiency**

1082 **A**, Breeding strategy for generation of mice gene-targeted for Vmat2 in VTA NEX-Cre
1083 neurons. NEX-Cre transgenic mice were mated to $Vmat2^{lox/lox}$ mice to generate NEX-Cre-
1084 positive mice homozygous for $Vmat2^{lox/lox}$ ($Vmat2^{lox/lox};NEX-Cre-tg$: cKO mice) and littermate
1085 control mice homozygous for $Vmat2^{lox/lox}$ and negative for the NEX-Cre transgene
1086 ($Vmat2^{lox/lox};NEX-Cre-wt$: Ctrl mice). **B**, 2-probe approach for detection of Vmat2 mRNA by *in*
1087 *situ* hybridization. Probe 1 detects exons 6-15 and Probe 2 detects exon 2 of the Vmat2 gene.
1088 Exon 2 is floxed in $Vmat2^{lox/lox}$ mice leading to failure of Probe 2-binding to Vmat2 mRNA in
1089 cKO neurons. **C**, Implementation of Vmat2 mRNA 2-probe approach in $Vmat2^{lox/lox};NEX-Cre-wt$
1090 (Ctrl, left panel) and $Vmat2^{lox/lox};NEX-Cre-tg$ (cKO, right panel) brains. Wildtype neurons are
1091 positive for both Vmat2 probes, while cKO neurons are only positive for Probe 1 due to
1092 targeted deletion of exon 2 (detected by Probe 2). Probe 1 detected in green and Probe 2
1093 detected in blue results in green-blue double-labeling in wild-type cells and green-only
1094 labeling in cKO cells. Green arrows point to green-only cells, i.e. VMAT2 cKO cells. **D**,
1095 Vmat2 mRNA 2-probe *in-situ* hybridization in additional monoaminergic areas. **E**, TH
1096 immunohistochemistry in Ctrl and cKO midbrain and striatum.
1097 Abbreviations: LC, locus coeruleus; ROB, raphe nucleus obscurus; VMH, ventromedial
1098 hypothalamus; VTA, ventral tegmental area; SNc, substantia nigra *pars compacta*; DStr,
1099 dorsal striatum; NAc, nucleus accumbens; OT, olfactory tubercle.

1100 **Figure 3. Altered responsiveness to psychostimulants upon ablation of Vmat2 gene**
1101 **expression in NeuroD6 VTA neurons**

1102 Color coding: $Vmat2^{lox/lox};NEX-Cre-wt$ (Ctrl) in white; $Vmat2^{lox/lox};NEX-Cre-tg$ (cKO) in green. **A**,
1103 Weight curve for Ctrl (N=14) and cKO (N=23) mice. Data presented as mean weight in grams
1104 for each week \pm SEM (+ $p<0.05$ effect of genotype; ### $p<0.001$, effect of age). **B**, Baseline
1105 locomotion in novel environment. Ctrl (N=17) and cKO (N=17). Data expressed as mean
1106 distance moved in 5 min bins \pm SEM (### $p<0.001$, effect of time). **C**, Sucrose preference

1107 expressed as percentage of preference for sucrose over tap water \pm SEM. Ctrl (N=14) and
1108 cKO (N=21). (### p <0.001 effect of sucrose concentration). **D**, Ethanol preference expressed
1109 as percentage of preference for ethanol solution over tap water \pm SEM. Ctrl (N=14) and cKO
1110 (N=14) (### p <0.001 effect of ethanol concentration, §§§ p <0.001 3% vs 6% and 10% in ctrl
1111 mice). **E**, Cocaine-induced locomotion. Top: Administration schedule. Bottom: Average
1112 distance moved 1 hour post-injection of saline and 5, 10, 20 mg/kg of cocaine; Ctrl (N=14)
1113 and (N=21) mice. Data expressed as total distance moved during the 1h recording period \pm
1114 SEM. (### p <0.001 effect of session). **F**, Amphetamine-induced locomotion. Top:
1115 Administration schedule. Bottom: Average distance moved 1.5 hours post-injection; Ctrl
1116 (N=17) and cKO mice (N=17). Data presented as mean of total distance moved in cm \pm SEM
1117 for each session ++ p <0.01 effect of genotype, ### p <0.001 effect of session, * p <0.05 & ***
1118 p <0.001 cKO vs Ctrl). **G**, Conditioned place preference (CPP). Illustration of setup and
1119 administration schedule. **H & J**, Preference score displayed as Δ sec, the difference between
1120 time spent in drug-paired compared during pretest and test \pm SEM, positive value indicates
1121 preference (cocaine: Ctrl N=12, cKO N=15; amphetamine: Ctrl N=13, cKO N=16). **I & K**,
1122 Cocaine- and amphetamine-induced locomotion during conditioning in the CPP setup
1123 displayed as distance moved in 30 min \pm SEM (cocaine: Ctrl N=12, cKO N=15;
1124 amphetamine: Ctrl N=15, cKO N=17, + p =0.031 effect of genotype, ## p =0.006, ### p <0.001
1125 effect of session).

1126

1127 **Figure 4 NeuroD6 mRNA co-localizes partly with Calb2 mRNA, but Calb2 mRNA is**
1128 **abundant throughout VTA and SNc**

1129 Double-labeling fluorescent *in situ* hybridization in the ventral midbrain of adult wild-type
1130 mice detecting the following mRNAs: **A**, NeuroD6 (red) and Calb2 (green), inset with high-
1131 magnification of overlap (yellow), pie charts illustrating quantification of overlap between

1132 NeuroD6 and Calb2; **B**, Calb (red) and Th (green), inset with high-magnification of overlap
1133 (yellow), pie charts illustrating quantification of overlap between Th and Calb2; **C**, Calb2
1134 (red) and Dat (green), inset with high-magnification of Dat/Calb2 mRNA overlap (yellow),
1135 pie chart illustrating quantification of overlap between Th and Calb2; **D**, Calb2 (red) and
1136 Vglut2 (green), inset with high-magnification of Vglut2/Calb2 mRNA overlap (yellow) in
1137 blue square and Vglut2-negative/Calb2-positive (red) in white square, pie chart illustrating
1138 quantification of overlap between Th and Calb2; **E**, Calb2 (red) and Viaat (green), inset with
1139 high-magnification of Viaat negative or positive (red, yellow, green) in white square.

1140 Abbreviations: VTA, ventral tegmental area; SNc, substantia nigra *pars compacta*; PBP,
1141 parabrachial pigmented nucleus; PN, paranigral nucleus; PIF, parainterfascicular nucleus;
1142 RLi, rostral linear nucleus; IF, interfascicular nucleus.

1143

1144 **Figure 5. Spatially restricted striatal innervation by NeuroD6 and Calb2 VTA neurons**

1145 **A**, Schematic illustration of stereotaxic injection into VTA of Cre-dependent *DIO-ChR2-*
1146 *eYFP* DNA construct packaged into AAV. **B**, Representative VTA neurons immunopositive
1147 for TH (red), YFP (green) or both (yellow) (*DIO-ChR2-eYFP*-injected NEX-Cre mice). **C-F**,
1148 Representative pictures of VTA (left panels) and striatal complex (right panels) in *DIO-ChR2-*
1149 *eYFP*-injected DAT-Cre (**C-C'**); Vglut2-Cre (**D-D'**); Calb2-Cre (**E-E'**); NEX-Cre (**F-F'**)
1150 mice. Panel far right: Schematic summary of striatal innervation pattern. Additional target
1151 areas listed in *Table 1*. **G-F**. Quantification of YFP and TH immunofluorescent overlap:
1152 Schematic illustration of 4 representative VTA areas selected for counting, shown as squares
1153 and labeled VTA 1-4 (**G**); Results of quantifications shown in histograms for each VTA area
1154 and the total sum (**H**).

1155 Abbreviations: PBP, parabrachial pigmented nucleus; PN, paranigral nucleus; PIF,
1156 parainterfascicular nucleus; RLi, rostral linear nucleus; IF, interfascicular nucleus; SNc,

1157 substantia nigra *pars compacta*; SNr, substantia nigra *pars reticulata*, IPR: interpeduncular
1158 nucleus, rostral subnucleus; IPC: interpeduncular nucleus, caudal subnucleus; DMStr,
1159 dorsomedial striatum; NAcC, nucleus accumbens core; NAcSh, nucleus accumbens shell; aca;
1160 anterior commissure, anterior part; OT, olfactory tubercle.

1161

1162 **Figure 6 Optogenetic stimulation in striatal target areas of NeuroD6 and Calb2 VTA**
1163 **neurons verifies DA release**

1164 **A**, Schematic representation of stereotaxic injection into VTA of Cre-dependent *DIO-ChR2-*
1165 *eYFP* and *DIO-eYFP* (Ctrl); FSCV recording sites within NAcSh and OT (red dots). **B**.
1166 Illustration of the experimental setup. **C**, Representative light-evoked dopamine recordings
1167 from injected DAT-Cre (left), NEX-Cre (middle) and Calb2-Cre (right) mice in the NAcSh
1168 (top) and the OT (bottom). **D**, Quantification of photostimulation-evoked dopamine release in
1169 the NAc shell (left) and OT (right). N=10 recording sites per group for each region. Mice used
1170 for the recordings: DAT-Cre/ChR2 N=2, DAT-Cre/eYFP N=2, NEX-Cre/ChR2 N=3, NEX-
1171 Cre/ eYFP N=2 Calb2-Cre/ChR2 N=3, Calb2-Cre/eYFP N=2. Box-and-whisker plots: Center
1172 lines indicate medians, box edges represent the interquartile range, whiskers extend to the
1173 minimal and maximal values (*p<0.05, **p<0.01, ***p<0.001 ChR2 vs ctrl).

1174 Abbreviations: DStr, dorsal striatum; NAcSh, nucleus accumbens shell; OT, olfactory
1175 tubercle.

1176

1177 **Figure 7. Optogenetic stimulation in striatal target areas of NeuroD6 and Calb2 VTA**
1178 **neurons reveals glutamatergic post-synaptic responses.**

1179 **A**, Representative picture from patch-clamp slice electrophysiology in NAcSh of NEX-Cre
1180 mice and OT of Calb2-Cre mice injected with *DIO-ChR2-eYFP*. **B**. Representative traces of
1181 photostimulation-evoked post synaptic currents recorded from NAcSh cells from NEX-Cre

1182 and OT cells from Calb2-Cre mice injected with *DIO-ChR2-eYFP*. **C.** Pie charts represent the
1183 percentage of cells showing excitatory post synaptic currents (white) vs negative (black) upon
1184 photostimulation of terminals in the NAcSh (N=18 cells from 4 mice) of NEX-Cre mice, and
1185 OT (N=14 cells from 4 mice) of Calb2-Cre mice. The y axis shows amplitude in pA; each
1186 circle represents one cell and bold lines the mean amplitude \pm SEM. **D.** Patch-clamp
1187 recordings pre-(control) and post-bath application of DNQX upon photostimulation in NAcSh
1188 of NEX-Cre/ChR2 (left, N=6 cells from 3 mice) and OT of Calb2-Cre/ChR2 mice (right, N=5
1189 cells from 3 mice). Each circle represents one cell (* $p < 0.05$ control vs DNQX).

1190 Abbreviations: NAcSh, Nucleus accumbens shell; OT, Olfactory tubercle

1191

1192

1193 **Figure 8. Optogenetic activation of NeuroD6 VTA neurons, but not Calb2 VTA neurons,**
1194 **induces place preference**

1195 **A,** Schematic drawing of stereotaxic injection into VTA of Cre-dependent *DIO-ChR2-eYFP*,
1196 and of experimental setup for real-time place preference (RT-PP) analysis. **B-F.** Time spent in
1197 light-paired (blue), unpaired (white during Phase 1, black during Reversal Phase) and neutral
1198 (gray) compartments shown as mean percentage of time spent in each compartment \pm SEM
1199 (left) (* $p < 0.05$, *** $p < 0.001$ paired vs unpaired compartment); average percentage of time
1200 spent in each compartment during days 3,4,6 & 7 \pm SEM (bar graphs; right) (* $p < 0.05$, ***
1201 $p < 0.001$ vs light-paired compartment; # $p < 0.05$, ## $p < 0.01$, ### $p < 0.001$ vs unpaired
1202 compartment). DAT-Cre N=10; Vglut2-Cre N=7; Calb2-Cre N=7; NEX-Cre N=5. **F.** High-
1203 power stimulation of bilaterally injected NEX-Cre mice (N=4). **G.** Schematic illustration of
1204 optical fiber placement in mice analyzed in RT-PP analysis.

1205 Abbreviation: NS, non-significant.

1206

1207 **Table 1. Statistical analysis of results obtained in behavioral and electrophysiological**
1208 **experiments.**

1209

1210 **Table 2. Projection areas of VTA neurons represented in NEX-Cre and Calb2-Cre mice**
1211 **compared with DAT-Cre and Vglut2-Cre mice.** Summary of projection areas for VTA

1212 neurons virally injected with optogenetic constructs (*DIO-ChR2-eYFP*) in DAT-Cre, Vglut2-
1213 Cre, Calb2-Cre and NEX-Cre mice, respectively, and detected as YFP-positive fibers.

1214 + indicates presence of YFP-positive fibers; - indicates absence of YFP-positive fibers; (+)
1215 indicates low presence of fibers.

1216

1217 **Figure 2-1 *In situ* hybridization for detection of Th, NeuroD6 and Vmat2 mRNA.**

1218 Analysis of Th, NeuroD6 and Vmat2 (two probes, covering mRNA derived from exon 1 and
1219 exon 2, respectively) mRNAs using radioactively labeled oligo-probes on sections throughout
1220 the whole brains of *Vmat2*^{lox/lox/NEX-Cre-wt} (Ctrl) and *Vmat2*^{lox/lox/NEX-Cre-tg} (cKO) mice.

1221

1222 **Figure 8-1. Complementary data from behavioral optogenetics.** DAT-Cre-negative mice

1223 injected with *DIO-ChR2-eYFP* (**A**) and DAT-Cre-positive mice injected with *DIO-eYFP* mice
1224 (**B**) did not show preference to the light paired compartment so their results were pooled

1225 together (**C**). **D**. Schematic illustration of optical fiber placement for mice analyzed in RT-PP

1226 analysis. **E-G**. RT-PP testing under high power (20mW, 5ms, 20Hz) stimulation for DAT-

1227 Cre/ChR2 (**E**), Calb2-Cre/ChR2 (**F**) and NEX-Cre/ChR2 (**G**). **H**. RT-PP results for bilaterally

1228 injected NEX-Cre/ChR2 mice. (**A-C**, **E-H**: graphs: *p<0.05, **p<0.01, ***p<0.001 paired vs
1229 unpaired; bar graphs, *p<0.05, ***p<0.001 vs paired, # p<0.05, ### p<0.001 vs unpaired). **I**.

1230 Vglut2-Cre/ChR2 tested in the Neutral Compartment Preference (NCP) test. **ii**. Schematic of

1231 the experimental setup. **iii-iii**. Mice spent significantly more time in the light-unpaired neutral

1232 compartment (* $p < 0.05$, ** $p < 0.01$, *** $p < 0.001$ neutral vs Paired1 and Paired2 compartments).
1233 (DAT-Cre negative N=3, DAT-Cre/eYFP=3, DAT-Cre/ChR2 high power N=4, Calb2-
1234 Cre/ChR2 high power N=7, NEX-Cre/ChR2 N=4, NEX-Cre/ChR2 bilateral N=4).

1235 Abbreviation: NS, non-significant.

1236

1237 **References**

1238 Baik, J.-H. (2013). Dopamine Signaling in reward-related behaviors. *Front. Neural Circuits* 7:
1239 1–16.

1240 Beier, K.T., Steinberg, E.E., Deloach, K.E., Xie, S., Miyamichi, K., Schwarz, L., Gao, X.J., Kremer,
1241 E.J., Malenka, R.C., and Luo, L. (2015). Circuit Architecture of VTA Dopamine Neurons
1242 Revealed by Systematic Input-Output Mapping. *Cell* 162: 622–634.

1243 Björklund, A., and Dunnett, S.B. (2007). Dopamine neuron systems in the brain: an update.
1244 *Trends Neurosci.* 30: 194–202.

1245 Borgius, L., Restrepo, C.E., Leao, R.N., Saleh, N., and Kiehn, O. (2010). A transgenic mouse
1246 line for molecular genetic analysis of excitatory glutamatergic neurons. *Mol. Cell. Neurosci.*
1247 45: 245–257.

1248 Brichta, L., and Greengard, P. (2014). Molecular determinants of selective dopaminergic
1249 vulnerability in Parkinson's disease: an update. *Front. Neuroanat.* 8: 152.

1250 Cenci, M.A., Francardo, V., O'Sullivan, S.S., and Lindgren, H.S. (2015). Rodent models of
1251 impulsive-compulsive behaviors in Parkinson's disease: How far have we reached?
1252 *Neurobiol. Dis.* 82: 561-573.

1253 Di Chiara, G., and Bassareo, V. (2007). Reward system and addiction: what dopamine does
1254 and doesn't do. *Curr. Opin. Pharmacol.* 7: 69–76.

1255 Chung, C.Y., Seo, H., Sonntag, K.C., Brooks, A., Lin, L., and Isacson, O. (2005). Cell type-

1256 specific gene expression of midbrain dopaminergic neurons reveals molecules involved in
1257 their vulnerability and protection. *Hum. Mol. Genet.* 14: 1709–1725.

1258 Deisseroth, K. (2015). Optogenetics: 10 years of microbial opsins in neuroscience. *Nat.*
1259 *Neurosci.* 18: 1213–1225.

1260 Divac, N., Prostran, M., Jakovcevski, I., and Cerovac, N. (2014). Second-generation
1261 antipsychotics and extrapyramidal adverse effects. *Biomed Res. Int.* 2014:656370.

1262 Ekstrand, M.I., Terzioglu, M., Galter, D., Zhu, S., Hofstetter, C., Lindqvist, E., Thams, S.,
1263 Bergstrand, A., Hansson, F.S., Trifunovic, A., et al. (2007). Progressive parkinsonism in mice
1264 with respiratory-chain-deficient dopamine neurons. *Proc. Natl. Acad. Sci.* 104: 1325–1330.

1265 Faget, L., Osakada, F., Duan, J., Ressler, R., Johnson, A.B., Proudfoot, J.A., Yoo, J.H., Callaway,
1266 E.M., and Hnasko, T.S. (2016). Afferent Inputs to Neurotransmitter-Defined Cell Types in the
1267 Ventral Tegmental Area. *Cell Rep.* 15: 2796–2808.

1268 Franklin, K.B.J., and Paxinos, G. (2008). The mouse brain in stereotaxic coordinates 3rd
1269 *Edition*. Boston: Academic Press.

1270 Fu, Y.H., Yuan, Y., Halliday, G., Rusznák, Z., Watson, C., and Paxinos, G. (2012). A
1271 cytoarchitectonic and chemoarchitectonic analysis of the dopamine cell groups in the
1272 substantia nigra, ventral tegmental area, and retrorubral field in the mouse. *Brain Struct.*
1273 *Funct.* 217: 591–612.

1274 Goebbels, S., Bormuth, I., Bode, U., Hermanson, O., Schwab, M.H., and Nave, K.-A. (2006).
1275 Genetic targeting of principal neurons in neocortex and hippocampus of NEX-Cre mice.
1276 *Genesis* 44: 611–621.

1277 Greene, J.G., Dingledine, R., and Greenamyre, J.T. (2005). Gene expression profiling of rat
1278 midbrain dopamine neurons: Implications for selective vulnerability in parkinsonism.
1279 *Neurobiol. Dis.* 18: 19–31.

- 1280 Hnasko, T.S., Hjelmstad, G.O., Fields, H.L., and Edwards, R.H. (2012). Ventral Tegmental Area
1281 Glutamate Neurons: Electrophysiological Properties and Projections. *J. Neurosci.* 32: 15076–
1282 15085.
- 1283 Hook, P.W., McClymont, S.A., Cannon, G.H., Law, W.D., Morton, A.J., Goff, L.A., and
1284 McCallion, A.S. (2018). Single-Cell RNA-Seq of Mouse Dopaminergic Neurons Informs
1285 Candidate Gene Selection for Sporadic Parkinson Disease. *Am. J. Hum. Genet.* 102, 427–446.
- 1286 Hopman, A.H.N., Ramaekers, F.C.S., and Speel, E.J.M. (1998). Rapid Synthesis of Biotin-,
1287 Digoxigenin-, Trinitrophenyl-, and Fluorochrome-labeled Tyramides and Their Application for
1288 In Situ Hybridization Using CARD Amplification. *J Histochem Cytochem.* 46: 771–777.
- 1289 Ikemoto, S. (2007). Dopamine reward circuitry: Two projection systems from the ventral
1290 midbrain to the nucleus accumbens-olfactory tubercle complex. *Brain Res. Rev.* 56: 27–78.
- 1291 Ikemoto, S., and Bonci, A. (2014). Neurocircuitry of drug reward. *Neuropharmacology.* 76:
1292 329-341.
- 1293 Ilango, A., Kesner, A.J., Broker, C.J., Wang, D. V., and Ikemoto, S. (2014). Phasic excitation of
1294 ventral tegmental dopamine neurons potentiates the initiation of conditioned approach
1295 behavior: parametric and reinforcement-schedule analyses. *Front. Behav. Neurosci.* 8: 155.
- 1296 Isingrini, E., Perret, L., Rainer, Q., Sagueby, S., Moquin, L., Gratton, A., and Giros, B. (2016).
1297 Selective genetic disruption of dopaminergic, serotonergic and noradrenergic
1298 neurotransmission: Insights into motor, emotional and addictive behaviour. *J. Psychiatry*
1299 *Neurosci.* 41: 169–181.
- 1300 Kalivas, P.W., Striplin, C.D., Steketee, J.D., Klitenick, M. a, and Duffy, P. (1992). Cellular
1301 mechanisms of behavioral sensitization to drugs of abuse. *Ann. N. Y. Acad. Sci.* 654: 128–
1302 135.
- 1303 Khan, S., Stott, S.R.W., Chabrat, A., Truckenbrodt, A.M., Spencer-Dene, B., Nave, K.-A.,

- 1304 Guillemot, F., Levesque, M., and Ang, S.-L. (2017). Survival of a Novel Subset of Midbrain
1305 Dopaminergic Neurons Projecting to the Lateral Septum Is Dependent on NeuroD Proteins. *J.*
1306 *Neurosci.* 37: 2305–2316.
- 1307 Kim, K.M., Baratta, M. V., Yang, A., Lee, D., Boyden, E.S., and Fiorillo, C.D. (2012).
1308 Optogenetic mimicry of the transient activation of dopamine neurons by natural reward is
1309 sufficient for operant reinforcement. *PLoS One* 7: 1–8.
- 1310 Kramer, D.J., Risso, D., Kosillo, P., Ngai, J., and Bateup, H.S. (2018). Combinatorial Expression
1311 of Grp and Neurod6 Defines Dopamine Neuron Populations with Distinct Projection Patterns
1312 and Disease Vulnerability. *eNeuro* 5.
- 1313 Lammel, S., Ion, D.I., Roeper, J., and Malenka, R.C. (2011). Projection-Specific Modulation of
1314 Dopamine Neuron Synapses by Aversive and Rewarding Stimuli. *Neuron* 70: 855–862.
- 1315 Lammel, S., Lim, B.K., Ran, C., Huang, K.W., Betley, M.J., Tye, K.M., Deisseroth, K., and
1316 Malenka, R.C. (2012). Input-specific control of reward and aversion in the ventral tegmental
1317 area. *Nature* 491: 212–217.
- 1318 Lammel, S., Steinberg, E.E., Földy, C., Wall, N.R., Beier, K., Luo, L., and Malenka, R.C. (2015).
1319 Diversity of transgenic mouse models for selective targeting of midbrain dopamine neurons.
1320 *Neuron* 85: 429–438.
- 1321 Lindeberg, J., Usoskin, D., Bengtsson, H., Gustafsson, A., Kylberg, A., Söderström, S., and
1322 Ebendal, T. (2004). Transgenic expression of Cre recombinase from the tyrosine hydroxylase
1323 locus. *Genesis* 40: 67–73.
- 1324 La Manno, G., Gyllborg, D., Codeluppi, S., Nishimura, K., Salto, C., Zeisel, A., Borm, L.E., Stott,
1325 S.R.W., Toledo, E.M., Villaescusa, J.C., et al. (2016). Molecular Diversity of Midbrain
1326 Development in Mouse, Human, and Stem Cells. *Cell* 167: 566–580.
- 1327 Menegas, W., Bergan, J.F., Ogawa, S.K., Isogai, Y., Venkataraju, K.U., Osten, P., Uchida, N.,

1328 and Watabe-Uchida, M. (2015). Dopamine neurons projecting to the posterior striatum form
1329 an anatomically distinct subclass. *Elife* 4: 1–30.

1330 Morales, M., and Margolis, E.B. (2017). Ventral tegmental area: Cellular heterogeneity,
1331 connectivity and behaviour. *Nat. Rev. Neurosci.* 18: 73–85.

1332 Narboux-Nême, N., Sagné, C., Doly, S., Diaz, S.L., Martin, C.B.P., Angenard, G., Martres, M.P.,
1333 Giros, B., Hamon, M., Lanfumey, L., et al. (2011). Severe serotonin depletion after
1334 conditional deletion of the vesicular monoamine transporter 2 gene in serotonin neurons:
1335 Neural and behavioral consequences. *Neuropsychopharmacology* 36: 2538–2550.

1336 Nordenankar, K., Smith-Anttila, C.J.A., Schweizer, N., Viereckel, T., Birgner, C., Mejia-Toiber,
1337 J., Morales, M., Leao, R.N., and Wallén-Mackenzie, Å. (2015). Increased hippocampal
1338 excitability and impaired spatial memory function in mice lacking VGLUT2 selectively in
1339 neurons defined by tyrosine hydroxylase promoter activity. *Brain Struct. Funct.* 220: 2171-
1340 2190.

1341 Pascoli, V., Terrier, J., Hiver, A., and Lüscher, C. (2015). Sufficiency of Mesolimbic Dopamine
1342 Neuron Stimulation for the Progression to Addiction. *Neuron* 88: 1054–1066.

1343 Poulin, J.-F., Caronia, G., Hofer, C., Cui, Q., Helm, B., Ramakrishnan, C., Chan, C.S., Dombeck,
1344 D.A., Deisseroth, K., and Awatramani, R. (2018). Mapping projections of molecularly defined
1345 dopamine neuron subtypes using intersectional genetic approaches. *Nat. Neurosci.* 21:
1346 1260-1271.

1347 Poulin, J.F., Zou, J., Drouin-Ouellet, J., Kim, K.Y.A., Cicchetti, F., and Awatramani, R.B. (2014).
1348 Defining midbrain dopaminergic neuron diversity by single-cell gene expression profiling.
1349 *Cell Rep.* 9: 930–943.

1350 Pupe, S., and Wallén-Mackenzie, Å. (2015). Cre-driven optogenetics in the heterogeneous
1351 genetic panorama of the VTA. *Trends Neurosci.* 38: 375–386.

- 1352 Qi, J., Zhang, S., Wang, H.-L., Barker, D.J., Miranda-Barrientos, J., and Morales, M. (2016).
1353 VTA glutamatergic inputs to nucleus accumbens drive aversion by acting on GABAergic
1354 interneurons. *Nat. Neurosci.* 19: 725-733.
- 1355 Robinson, T.E., and Berridge, K.C. (1993). The neural basis of drug craving: An incentive-
1356 sensitization theory of addiction. *Brain Res. Rev.* 18: 247–291.
- 1357 Roeper, J. (2013). Dissecting the diversity of midbrain dopamine neurons. *Trends Neurosci.*
1358 36: 336–342.
- 1359 Root, D.H., Mejias-Aponte, C.A., Qi, J., and Morales, M. (2014). Role of Glutamatergic
1360 Projections from Ventral Tegmental Area to Lateral Habenula in Aversive Conditioning. *J.*
1361 *Neurosci.* 34: 13906–13910.
- 1362 Stamatakis, A.M., Jennings, J.H., Ung, R.L., Blair, G.A., Weinberg, R.J., Neve, R.L., Boyce, F.,
1363 Mattis, J., Ramakrishnan, C., Deisseroth, K., et al. (2013). A Unique Population of Ventral
1364 Tegmental Area Neurons Inhibits the Lateral Habenula to Promote Reward. *Neuron* 80:
1365 1039–1053.
- 1366 Stuber, G.D., Hnasko, T.S., Britt, J.P., Edwards, R.H., and Bonci, A. (2010). Dopaminergic
1367 Terminals in the Nucleus Accumbens But Not the Dorsal Striatum Corelease Glutamate. *J.*
1368 *Neurosci.* 30: 8229–8233.
- 1369 Stuber, G.D., Stamatakis, A.M., and Kantak, P.A. (2015). Considerations when using cre-
1370 driver rodent lines for studying ventral tegmental area circuitry. *Neuron* 85: 439-445.
- 1371 Trudeau, L.-E., and El Mestikawy, S. (2018). Glutamate Cotransmission in Cholinergic,
1372 GABAergic and Monoamine Systems: Contrasts and Commonalities. *Front. Neural Circuits*
1373 12: 113.
- 1374 Tsai, H.-C., Zhang, F., Adamantidis, A.R., Stuber, G.D., Bonci, A., de Lecea, L., and Deisseroth,
1375 K. (2009). Phasic firing in dopaminergic neurons is sufficient for behavioral conditioning.

- 1376 Science 324: 1080–1084.
- 1377 Viereckel, T., Dumas, S., Smith-Anttila, C.J.A., Vlcek, B., Bimpisidis, Z., Lagerström, M.C.,
1378 Konradsson-Geuken, Å., & Wallén-Mackenzie, Å. (2016). Midbrain Gene Screening Identifies
1379 a New Mesoaccumbal Glutamatergic Pathway and a Marker for Dopamine Cells
1380 Neuroprotected in Parkinson’s Disease. *Sci. Rep.* 6: 1–16.
- 1381 Wang, H.-L., Qi, J., Zhang, S., Wang, H., and Morales, M. (2015). Rewarding Effects of Optical
1382 Stimulation of Ventral Tegmental Area Glutamatergic Neurons. *J. Neurosci.* 35: 15948–
1383 15954.
- 1384 Weintraub, D. (2008). Dopamine and impulse control disorders in Parkinson’s disease. *Ann.*
1385 *Neurol.* 64: 93–100.
- 1386 Yoo, J.H., Zell, V., Gutierrez-Reed, N., Wu, J., Ressler, R., Shenasa, M.A., Johnson, A.B., Fife,
1387 K.H., Faget, L., and Hnasko, T.S. (2016). Ventral tegmental area glutamate neurons co-
1388 release GABA and promote positive reinforcement. *Nat. Commun.* 7: 1–13.
- 1389 Zhang, Z., Liu, Q., Wen, P., Zhang, J., Rao, X., Zhou, Z., Zhang, H., He, X., Li, J., Zhou, Z., et al.
1390 (2017). Activation of the dopaminergic pathway from VTA to the medial olfactory tubercle
1391 generates odor-preference and reward. *Elife* 6: 1–24.
- 1392

Figure	Data structure	Type of test	Sample Size	Statistical data
Figure 3A Weight analysis of ctrl and cKO mice	Normally distributed	Two-way ANOVA followed by Sidak's multiple comparison test	Ctrl N=14 (M=8, F=6) cKO N=23 (M=15, F=8)	Interaction: $p = 0.996$, $F_{(4,158)} = 0.0447$ Week: $p < 0.001$, $F_{(4,158)} = 79.8$ Genotype: $p = 0.032$, $F_{(1,158)} = 4.67$ Multiple comparisons Ctrl vs cKO w4 $p=0.908$; 95% CI: -3.55 to 1.75 w5 $p=0.966$; 95% CI: -2.70 to 1.57 w6 $p=0.876$; 95% CI: -2.91 to 1.35 w7 $p=0.720$; 95% CI: -3.19 to 1.15 w8 $p=0.783$; 95% CI: -3.11 to 1.23
Figure 3B Baseline locomotion of ctrl and cKO mice for 30 min in 5-min bins	Normally distributed	Two-way RM ANOVA followed by Sidak's multiple comparison test	Ctrl N=17 (M=8, F=9) cKO N=17 (M=13, F=4)	Interaction: $p = 0.256$, $F_{(5,160)} = 1.33$ Time: $p < 0.001$, $F_{(5,160)} = 69.5$ Genotype: $p = 0.535$, $F_{(1,32)} = 0.00912$ Multiple comparisons Ctrl vs cKO 5 $p>0.999$; 95% CI: -287 to 211 10 $p>0.999$; 95% CI: -217 to 282 15 $p=0.952$; 95% CI: -170 to 329 20 $p>0.999$; 95% CI: -236 to 263 25 $p=0.886$; 95% CI: -346 to 153 30 $p=0.993$; 95% CI: -195 to 304
Figure 3C Sucrose preference of ctrl and cKO mice for 1, 3 and 10% sucrose solutions	Normally distributed	Two-way RM ANOVA followed by Sidak's multiple comparison test	Ctrl N=14 (M=8, F=6) cKO N=21 (M=13, F=8)	Interaction: $p = 0.475$, $F_{(2,66)} = 0.752$ Concentration: $p < 0.001$, $F_{(2,66)} = 151$ Genotype: $p = 0.297$, $F_{(1,33)} = 1.12$ Multiple comparisons Ctrl vs cKO 1% $p>0.999$; 95% CI: -5.21 to 5.69 3% $p=0.294$; 95% CI: -1.83 to 9.08 10% $p=0.991$; 95% CI: -4.85 to 6.05
Figure 3D Ethanol preference of ctrl and cKO mice for 3, 6 and 10% ethanol concentrations	Normally distributed	Two-way RM ANOVA followed by Sidak's multiple comparison test	Ctrl N=14 (M=7, F=7) cKO N=14 (M=6, F=8)	Interaction: $p = 0.129$, $F_{(2,52)} = 2.13$ Concentration: $p < 0.001$, $F_{(2,52)} = 14.2$ Genotype: $p = 0.334$, $F_{(1,26)} = 0.969$ Multiple comparisons Ctrl vs cKO 3% $p=0.983$; 95% CI: -9.31 to 7.11 6% $p=0.453$; 95% CI: -3.68 to 12.7 10% $p=0.396$; 95% CI: -3.38 to 13.0 Ctrl 3% vs 6% $p<0.001$; 95% CI: -14.7 to -3.45 3% vs 10% $p<0.001$; 95% CI: -16.9 to -5.58 6% vs 10% $p=0.733$; 95% CI: -7.78 to 3.52 cKO 3% vs 6% $p=0.354$; 95% CI: -9.11 to 2.18 3% vs 10% $p=0.072$; 95% CI: -10.9 to 0.354 6% vs 10% $p=0.814$; 95% CI: -7.47 to 3.82
Figure 3E Injection-induced locomotion for ctrl and cKO mice after saline and 5,10 & 20 mg/kg injections of cocaine	Normally distributed	Two-way RM ANOVA followed by Sidak's multiple comparison test	Ctrl N=14 (M=8, F=6) cKO N=21 (M=13, F=8)	Interaction: $p = 0.396$, $F_{(3,99)} = 1$ Session: $p<0.001$, $F_{(3,99)} = 108$ Genotype: $p = 0.208$, $F_{(1,33)} = 1.65$ Multiple comparisons Ctrl vs cKO Saline $p=0.966$; 95% CI: -3437 to 5436 5 mg/kg. $p=0.962$; 95% CI: -3410 to 5464 10 mg/kg. $p=0.887$; 95% CI: -3015 to 5858 20 mg/kg. $p=0.152$; 95% CI: -802 to 8071
Figure 3F Amphetamine-induced (3 mg/kg) locomotion under a sensitization protocol for ctrl and cKO mice	Normally distributed	Two-way RM ANOVA followed by Sidak's multiple comparison test	Ctrl N=17 (M=8, F=9) cKO N=17 (M=13, F=4)	Interaction: $p<0.001$, $F_{(5,160)} = 4.79$ Session: $p<0.001$, $F_{(5,160)} = 40.9$ Genotype: $p = 0.005$, $F_{(1,32)} = 9.09$ Multiple comparisons Ctrl vs cKO Day1 $p>0.999$; 95% CI: -13977 to 12091 Day2 $p=0.266$; 95% CI: -3371 to 22696 Day3 $p=0.063$; 95% CI: -407 to 25661

				Day4 $p=0.011$; 95% CI: -2481 to 28549 Day5 $p<0.001$; 95% CI: -6873 to 32941 Day17 $p=0.029$; 95% CI: -928 to 26996
Figure 3H (top panel) Cocaine (20 mg/kg, i.p) CPP for ctrl and cKO mice	Normally distributed	Unpaired t-test	Ctrl N=12 (M=6, F=6) cKO N=15 (M=6, F=9)	t-test ctrl vs cKO $p=0.860$; 95% CI: -162.0 to 136.1
Figure 3H (bottom panel) Amphetamine (3 mg/kg, i.p.) CPP for ctrl and cKO mice	Assumed normality	Unpaired t-test	Ctrl N=13 (M=6, F=7) cKO N=16 (M=9, F=7)	t-test ctrl vs cKO $p=0.744$; 95% CI: -365.5 to 264.3
Figure 3I (top panel) Cocaine-induced locomotion during the CPP for ctrl and cKO mice	Assumed normality	Two-way RM ANOVA followed by Sidak's multiple comparison test	Ctrl N=12 (M=6, F=6) cKO N=15 (M=6, F=9)	Interaction: $p=0.652$, $F_{(3,75)} = 0.5$ Session: $p=0.006$, $F_{(3,75)} = 4.4$ Genotype: $p = 0.031$, $F_{(1,25)} = 5.2$ Multiple comparisons Ctrl vs cKO Injection 1: $p=0.373$; 95% CI: -6850 to 1526 Injection 2: $p=0.067$; 95% CI: -8185 to 191 Injection 3: $p=0.115$; 95% CI: -7818 to 558 Injection 4: $p=0.475$; 95% CI: -6591 to 1785
Figure 3I (bottom panel) Amphetamine- induced locomotion during the CPP for ctrl and cKO mice	Normally distributed	Mixed-effects model (REML) followed by Sidak's multiple comparison test	Ctrl N=15 (M=7, F=8) cKO N=17 (M=10, F=7)	Interaction: $p=0.567$, $F_{(3,85)} = 0.680$ Session: $p<0.001$, $F_{(3,85)} = 24.0$ Genotype: $p = 0.803$, $F_{(1,30)} = 0.0631$ Multiple comparisons Ctrl vs cKO Injection 1: $p=0.941$; 95% CI: -2522 to 1473 Injection 2: $p=0.931$; 95% CI: -1431 to 2517 Injection 3: $p=0.995$; 95% CI: -1783 to 2331 Injection 4: $p=0.989$; 95% CI: -1671 to 2327
Figure 6D (left) Optically evoked DA release in NAcSh of DAT-, NEX- and Calb2-Cre mice injected with Chr2 or eYFP	Normally distributed	Unpaired t-test	10 observations for each group and virus DAT-Cre/Chr2 N=2 (M=0, F=2) DAT-Cre/eYFP N=2 (M=1, F=1) NEX-Cre/Chr2 N=3 (M=2, F=1) NEX-Cre/eYFP N=2 (M=0, F=2) Calb2-Cre/Chr2 N=3 (M=1, F=2) Calb2-Cre/eYFP N=2 (M=0, F=2)	t-test DAT-Cre/Chr2 vs DAT-Cre/eYFP $p<0.0001$; 95% CI: -1.272 to -0.6540 NEX-Cre/Chr2 vs NEX-Cre/eYFP $p<0.0001$; 95% CI: -0.6289 to -0.2909 Calb2-Cre/Chr2 vs Calb2-Cre/eYFP $p=0.0148$; 95% CI: -0.01602 to -0.001988
Figure 6D (right) Optically evoked DA release in OT of DAT-, NEX- and Calb2-Cre mice injected with Chr2 or eYFP	Normally distributed	Unpaired t-test	As above	t-test DAT-Cre/Chr2 vs DAT-Cre/eYFP $p<0.0001$; 95% CI: -0.2354 to -0.1810 NEX-Cre/Chr2 vs NEX-Cre/eYFP $p=0.0049$; 95% CI: -0.01295 to -0.002704

				Calb2-Cre/ChR2 vs Calb2-Cre/eYFP $p=0.0002$; 95% CI: -0.02022 to -0.007554
Figure 7D (left panel) Optically evoked EPSCs in NAcSh of NEX-Cre/ChR2 mice before (control) and after DNQX bath application	Assumed normality	Paired t-test	6 cells from 3 NEX-Cre/ChR2 mice (M=3, F=0)	$p=0.0481$; 95% CI: -61.86 to -0.3739
Figure 7D (right panel) Optically evoked EPSCs in OT of Calb2-Cre/ChR2 mice before (control) and after DNQX bath application	Assumed normality	Paired t-test	5 cells from 3 Calb2-Cre/ChR2 mice (M=2, F=1)	$p=0.0456$; 95% CI: -89.88 to -1.444
Figure 8B (left) Behavioral analysis of DAT-Cre/ChR2 mice throughout the opto-behavioral experiments	Normally distributed	Two-way RM ANOVA followed by Tukey's multiple comparison test	N=10 (M=2, F=8)	Interaction: $p < 0.001$, $F_{(12,108)} = 33$ Day: $p = 0.435$, $F_{(6,54)} = 1$ Compartment: $p < 0.001$, $F_{(2,18)} = 51.8$ Multiple comparisons (of interest) Day2 (Pre-test) Paired vs Unpaired $p=0.513$; 95% CI: -38.4 to -6.29 Day3 (RT-PP) Paired vs Unpaired $p<0.001$; 95% CI: 21.7 to 66.4 Paired vs neutral $p<0.001$; 95% CI: 35.7 to 80.4 Day4 (RT-PP) Paired vs Unpaired $p<0.001$; 95% CI: 37.6 to 82.3 Paired vs neutral $p<0.001$; 95% CI: 47.3 to 92.0 Day5 (CR) Paired vs Unpaired $p<0.001$; 95% CI: 11.5 to 56.1 Paired vs neutral $p<0.001$; 95% CI: 26.7 to 71.4 Day6 (RT-PP) Paired vs Unpaired $p<0.001$; 95% CI: -65.7 to -21.0 Paired vs neutral $p<0.001$; 95% CI: 34.4 to 79.1 Day7 (RT-PP) Paired vs Unpaired $p<0.001$; 95% CI: -85.0 to -40.4 Paired vs neutral $p<0.001$; 95% CI: 43.1 to 87.7 Day8 (CR) Paired vs Unpaired $p<0.001$; 95% CI: -67.2 to -22.5 Paired vs neutral $p<0.001$; 95% CI: 33.6 to 78.3 Reversal parameters: Day3 paired vs Day6 unpaired $p<0.001$; 95% CI: 22.8 to 67.4 Day3 paired vs Day7 unpaired $p<0.001$; 95% CI: 32.5 to 77.2 Day4 paired vs Day6 unpaired $p<0.001$; 95% CI: 32.3 to 76.9 Day4 paired vs Day7 unpaired $p<0.001$; 95% CI: 42.0 to 86.7 Day5 paired vs Day8 unpaired $p<0.001$; 95% CI: 17.5 to 62.2
Figure 8B (right) time spent in paired, unpaired and neutral compartments during the 4 RT-PP days for DAT-Cre/ChR2 mice	Normally distributed	RM One-Way ANOVA followed by Tukey's multiple comparison test	N=10 (M=2, F=8)	Compartment $p < 0.001$, $F_{(2,6)} = 166$ Multiple comparisons Paired vs unpaired $p<0.001$; 95% CI: 41.1 to 63.9 Paired vs neutral $p<0.001$; 95% CI: 51.7 to 74.5 Unpaired vs neutral $p=0.066$; 95% CI: -0.808 to 22.0
Figure 8-1A (left) Behavioral analysis of DAT-Cre negative mice injected with AAV-ChR2 throughout the opto-behavioral experiments	Normally distributed	Two-way RM ANOVA followed by Tukey's multiple comparison test	N=3 (M=0, F=3)	Interaction: $p = 0.562$, $F_{(12,24)} = 0.898$ Day: $p = 0.569$, $F_{(6,12)} = 0.830$ Compartment: $p = 0.102$, $F_{(2,4)} = 4.26$ Multiple comparisons (of interest) Day2 (Pre-test) Paired vs Unpaired $p=0.010$; 95% CI: -49.6 to -4.05 Day3 (RT-PP) Paired vs Unpaired $p=0.074$; 95% CI: 44.5 to 1.05 Paired vs neutral $p=0.292$; 95% CI: -5.3 to 40.3 Day4 (RT-PP) Paired vs Unpaired $p=0.236$; 95% CI: -41.0 to 4.57 Paired vs neutral $p=0.055$; 95% CI: -0.241 to 45.3 Day5 (CR) Paired vs Unpaired $p=0.074$; 95% CI: -44.5 to 1.08

				<p>Paired vs neutral $p=0.204$; 95% CI: -4.08 to 41.5</p> <p>Day6 (RT-PP)</p> <p>Paired vs Unpaired $p=0.998$; 95% CI: -30.3 to 15.3</p> <p>Paired vs neutral $p<0.001$; 95% CI: 12.0 to 57.6</p> <p>Day7 (RT-PP)</p> <p>Paired vs Unpaired $p=0.863$; 95% CI: -34.5 to 11.0</p> <p>Paired vs neutral $p=0.001$; 95% CI: 9.18 to 54.8</p> <p>Day8 (CR)</p> <p>Paired vs Unpaired $p=0.012$; 95% CI: -49.2 to -3.6</p> <p>Paired vs neutral $p<0.001$; 95% CI: 22.5 to 68.1</p> <p>Reversal parameters:</p> <p>Day3 paired vs Day6 unpaired $p=0.995$; 95% CI: -30.8 to 14.8</p> <p>Day3 paired vs Day7 unpaired $p>0.999$; 95% CI: -27.0 to 18.5</p> <p>Day4 paired vs Day6 unpaired $p>0.999$; 95% CI: -28.0 to 17.6</p> <p>Day4 paired vs Day7 unpaired $p>0.999$; 95% CI: -24.2 to 21.4</p> <p>Day5 paired vs Day8 unpaired $p>0.999$; 95% CI: -21.3 to 24.3</p>
<p>Figure 8-1A (right) time spent in paired, unpaired and neutral compartments during the 4 RT-PP days for DAT-Cre negative/Chr2 mice</p>	Normally distributed	RM One-Way ANOVA followed by Tukey's multiple comparison test	N=3 (M=0, F=3)	<p>Compartment $p < 0.001$, $F_{(2,6)} = 48.7$</p> <p>Multiple comparisons</p> <p>Paired vs unpaired $p=0.358$; 95% CI: -15.8 to 5.46</p> <p>Paired vs neutral $p<0.001$; 95% CI: 16.1 to 37.3</p> <p>Unpaired vs neutral $p<0.001$; 95% CI: 21.2 to 42.5</p>
<p>Figure 8-1B (left) Behavioral analysis of DAT-Cre/eYFP throughout the opto-behavioral experiments</p>	Normally distributed	Two-way RM ANOVA followed by Tukey's multiple comparison test	N=3 (M=0, F=3)	<p>Interaction: $p = 0.677$, $F_{(12,24)} = 0.767$</p> <p>Day: $p = 0.935$, $F_{(6,12)} = 0.281$</p> <p>Compartment: $p = 0.004$, $F_{(2,4)} = 27.9$</p> <p>Multiple comparisons (of interest)</p> <p>Day2 (Pre-test)</p> <p>Paired vs Unpaired $p<0.001$; 95% CI: -62.8 to -22.5</p> <p>Day3 (RT-PP)</p> <p>Paired vs Unpaired $p<0.001$; 95% CI: -64.9 to -24.6</p> <p>Paired vs neutral $p=0.198$; 95% CI: -3.52 to 36.7</p> <p>Day4 (RT-PP)</p> <p>Paired vs Unpaired $p<0.001$; 95% CI: -63.5 to -23.2</p> <p>Paired vs neutral $p=0.222$; 95% CI: -3.85 to 36.4</p> <p>Day5 (CR)</p> <p>Paired vs Unpaired $p<0.001$; 95% CI: -65.9 to -25.6</p> <p>Paired vs neutral $p=0.251$; 95% CI: -4.21 to 36.1</p> <p>Day6 (RT-PP)</p> <p>Paired vs Unpaired $p<0.001$; 95% CI: -70.7 to -30.5</p> <p>Paired vs neutral $p<0.001$; 95% CI: 45.8 to 86.1</p> <p>Day7 (RT-PP)</p> <p>Paired vs Unpaired $p<0.001$; 95% CI: -55.5 to -15.2</p> <p>Paired vs neutral $p<0.001$; 95% CI: 31.3 to 71.6</p> <p>Day8 (CR)</p> <p>Paired vs Unpaired $p<0.001$; 95% CI: -66.1 to -25.8</p> <p>Paired vs neutral $p<0.001$; 95% CI: -42.7 to 82.9</p> <p>Reversal parameters:</p> <p>Day3 paired vs Day6 unpaired $p>0.999$; 95% CI: -17.8 to 22.5</p> <p>Day3 paired vs Day7 unpaired $p>0.999$; 95% CI: -23.1 to 17.2</p> <p>Day4 paired vs Day6 unpaired $p>0.999$; 95% CI: -17.4 to 22.9</p> <p>Day4 paired vs Day7 unpaired $p>0.999$; 95% CI: -22.7 to 17.5</p> <p>Day5 paired vs Day8 unpaired $p>0.999$; 95% CI: -20.4 to 19.9</p>
<p>Figure 8-1B (right) time spent in paired, unpaired and neutral compartments during the 4 RT-PP days for DAT-Cre /eYFP mice</p>	Normally distributed	RM One-Way ANOVA followed by Tukey's multiple comparison test	N=3 (M=0, F=3)	<p>Compartment $p = 0.127$, $F_{(2,6)} = 2.97$</p> <p>Multiple comparisons</p> <p>Paired vs unpaired $p>0.999$; 95% CI: -55.6 to 54.5</p> <p>Paired vs neutral $p=0.171$; 95% CI: -17.5 to 92.6</p> <p>Unpaired vs neutral $p=0.165$; 95% CI: -16.9 to 93.1</p>
<p>Figure 8-1C (left) Behavioral analysis of DAT-Cre controls (pooled) throughout the opto-behavioral experiments</p>	Normally distributed	Two-way RM ANOVA followed by Tukey's multiple comparison test	N=6 (M=0, F=6)	<p>Interaction: $p = 0.494$, $F_{(12,60)} = 0.963$</p> <p>Day: $p = 0.929$, $F_{(6,30)} = 0.306$</p> <p>Compartment: $p < 0.001$, $F_{(2,10)} = 18.6$</p> <p>Multiple comparisons (of interest)</p> <p>Day2 (Pre-test)</p> <p>Paired vs Unpaired $p<0.001$; 95% CI: -48.6 to -20.8</p> <p>Day3 (RT-PP)</p>

				<p>Paired vs Unpaired $p < 0.001$; 95% CI: -47.1 to -19.4 Paired vs neutral $p = 0.004$; 95% CI: 3.15 to 30.9 Day4 (RT-PP) Paired vs Unpaired $p < 0.001$; 95% CI: -44.7 to -16.9 Paired vs neutral $p < 0.001$; 95% CI: 5.52 to 33.3 Day5 (CR) Paired vs Unpaired $p < 0.001$; 95% CI: -47.6 to -19.8 Paired vs neutral $p = 0.003$; 95% CI: 3.42 to 31.2 Day6 (RT-PP) Paired vs Unpaired $p < 0.001$; 95% CI: -42.9 to -15.1 Paired vs neutral $p < 0.001$; 95% CI: 36.5 to 64.3 Day7 (RT-PP) Paired vs Unpaired $p < 0.001$; 95% CI: -37.4 to -9.64 Paired vs neutral $p < 0.001$; 95% CI: 27.8 to 55.6 Day8 (CR) Paired vs Unpaired $p < 0.001$; 95% CI: -50.1 to -22.3 Paired vs neutral $p < 0.001$; 95% CI: 40.2 to 67.9 Reversal parameters: Day3 paired vs Day6 unpaired $p > 0.999$; 95% CI: -16.7 to 11.1 Day3 paired vs Day7 unpaired $p > 0.999$; 95% CI: -17.5 to 10.3 Day4 paired vs Day6 unpaired $p > 0.999$; 95% CI: -15.1 to 12.7 Day4 paired vs Day7 unpaired $p > 0.999$; 95% CI: -15.9 to 11.9 Day5 paired vs Day8 unpaired $p > 0.999$; 95% CI: -13.3 to 14.5</p>
<p>Figure 8-1C (right) time spent in paired, unpaired and neutral compartments during the 4 RT-PP days for DAT-Cre control mice (pooled)</p>	Normally distributed	RM One-Way ANOVA followed by Tukey's multiple comparison test	N=6 (M=0, F=6)	<p>Compartment $p = 0.015$, $F_{(2,6)} = 9.27$ Multiple comparisons Paired vs unpaired $p = 0.946$; 95% CI: -30.6 to 24.8 Paired vs neutral $p = 0.028$; 95% CI: 4.44 to 59.8 Unpaired vs neutral $p = 0.019$; 95% CI: 7.30 to 62.7</p>
<p>Figure 8-1E (left) Behavioral analysis of DAT-Cre/Chr2 mice tested on high power, throughout the opto-behavioral experiments</p>	Normally distributed	Two-way RM ANOVA followed by Tukey's multiple comparison test	N=10 (M=2, F=8)	<p>Interaction: $p < 0.001$, $F_{(12,36)} = 22.6$ Day: $p = 0.455$, $F_{(6,18)} = 1$ Compartment: $p < 0.001$, $F_{(2,6)} = 105$ Multiple comparisons (of interest) Day2 (Pre-test) Paired vs Unpaired $p > 0.999$; 95% CI: -45.7 to 26.7 Day3 (RT-PP) Paired vs Unpaired $p < 0.001$; 95% CI: 26.2 to 98.6 Paired vs neutral $p < 0.001$; 95% CI: 38.5 to 111 Day4 (RT-PP) Paired vs Unpaired $p < 0.001$; 95% CI: 42.7 to 115 Paired vs neutral $p < 0.001$; 95% CI: 47.1 to 119 Day5 (CR) Paired vs Unpaired $p < 0.001$; 95% CI: 17.4 to 89.8 Paired vs neutral $p < 0.001$; 95% CI: 16.5 to 88.8 Day6 (RT-PP) Paired vs Unpaired $p < 0.001$; 95% CI: -98.0 to -25.6 Paired vs neutral $p < 0.001$; 95% CI: 36.5 to 109 Day7 (RT-PP) Paired vs Unpaired $p < 0.001$; 95% CI: -109 to -37.0 Paired vs neutral $p < 0.001$; 95% CI: 42.3 to 115 Day8 (CR) Paired vs Unpaired $p = 0.407$; 95% CI: -62.5 to 9.72 Paired vs neutral $p = 0.030$; 95% CI: 1.98 to 74.3 Reversal parameters: Day3 paired vs Day6 unpaired $p < 0.001$; 95% CI: 26.5 to 98.9 Day3 paired vs Day7 unpaired $p < 0.001$; 95% CI: 32.1 to 104 Day4 paired vs Day6 unpaired $p < 0.001$; 95% CI: 34.8 to 107 Day4 paired vs Day7 unpaired $p < 0.001$; 95% CI: 40.5 to 113 Day5 paired vs Day8 unpaired $p < 0.001$; 95% CI: 4.15 to 76.5</p>
<p>Figure 8-1E (right) time spent in paired, unpaired and neutral compartments during the 4 RT-PP days for DAT-Cre/Chr2 mice under high</p>	Normally distributed	RM One-Way ANOVA followed by Tukey's multiple comparison test	N=4 (M=0, F=4)	<p>Compartment $p < 0.001$, $F_{(2,6)} = 404$ Multiple comparisons Paired vs unpaired $p < 0.001$; 95% CI: 59.9 to 78.2 Paired vs neutral $p < 0.001$; 95% CI: 68.1 to 86.5 Unpaired vs neutral $p = 0.074$; 95% CI: -0.934 to 17.4</p>

power stimulation Figure 8C (left) Behavioral analysis of Vglut2-Cre/Chr2 mice throughout the opto-behavioral experiments	Normally distributed	Two-way RM ANOVA followed by Tukey's multiple comparison test	N=7 (M=2, F=5)	Interaction: $p < 0.001$, $F_{(12,72)} = 16.1$ Day: $p = 0.181$, $F_{(6,36)} = 1.58$ Compartment: $p < 0.001$, $F_{(2,12)} = 40.9$ Multiple comparisons (of interest) Day2 (Pre-test) Paired vs Unpaired $p > 0.999$; 95% CI: -28.1 to 26.6 Day3 (RT-PP) Paired vs Unpaired $p < 0.001$; 95% CI: -71.9 to -17.2 Paired vs neutral $p > 0.999$; 95% CI: -18.0 to 36.7 Day4 (RT-PP) Paired vs Unpaired $p < 0.001$; 95% CI: -68.1 to -13.4 Paired vs neutral $p > 0.997$; 95% CI: -16.9 to 37.8 Day5 (CR) Paired vs Unpaired $p = 0.998$; 95% CI: -37.8 to 16.9 Paired vs neutral $p = 0.019$; 95% CI: 2.42 to 57.1 Day6 (RT-PP) Paired vs Unpaired $p < 0.001$; 95% CI: 32.9 to 87.6 Paired vs neutral $p > 0.999$; 95% CI: -28.8 to 25.9 Day7 (RT-PP) Paired vs Unpaired $p < 0.001$; 95% CI: 27.0 to 81.7 Paired vs neutral $p > 0.999$; 95% CI: -28.9 to 25.8 Day8 (CR) Paired vs Unpaired $p = 0.783$; 95% CI: -10.8 to 43.9 Paired vs neutral $p = 0.055$; 95% CI: -0.268 to 54.4 Reversal parameters: Day3 paired vs Day6 unpaired $p < 0.001$; 95% CI: -78.7 to -24.1 Day3 paired vs Day7 unpaired $p < 0.001$; 95% CI: -74.8 to -20.1 Day4 paired vs Day6 unpaired $p < 0.001$; 95% CI: -77.1 to -22.4 Day4 paired vs Day7 unpaired $p < 0.001$; 95% CI: -73.2 to -18.5 Day5 paired vs Day8 unpaired $p = 0.952$; 95% CI: -41.0 to 13.7
Figure 8C (right) time spent in paired, unpaired and neutral compartments during the 4 RT-PP days for Vglut2-Cre/Chr2 mice	Normally distributed	RM One-Way ANOVA followed by Tukey's multiple comparison test	N=7 (M=2, F=5)	Compartment $p < 0.001$, $F_{(2,6)} = 162$ Multiple comparisons Paired vs unpaired $p < 0.001$; 95% CI: -60.2 to -39.7 Paired vs neutral $p = 0.469$; 95% CI: -6.08 to 14.5 Unpaired vs neutral $p < 0.001$; 95% CI: 43.9 to 64.4
Figure 8D (left) Behavioral analysis of Calb2-Cre/Chr2 mice throughout the opto-behavioral experiments	Normally distributed	Two-way RM ANOVA followed by Tukey's multiple comparison test	N=7 (M=0, F=7)	Interaction: $p = 0.163$, $F_{(12,72)} = 1.45$ Day: $p = 0.567$, $F_{(6,36)} = 0.813$ Compartment: $p < 0.001$, $F_{(2,12)} = 27$ Multiple comparisons (of interest) Day2 (Pre-test) Paired vs Unpaired $p = 0.096$; 95% CI: -33.3 to 1.13 Day3 (RT-PP) Paired vs Unpaired $p = 0.343$; 95% CI: -30.6 to 3.82 Paired vs neutral $p = 0.010$; 95% CI: 2.52 to 37.0 Day4 (RT-PP) Paired vs Unpaired $p > 0.999$; 95% CI: -21.1 to 13.4 Paired vs neutral $p < 0.001$; 95% CI: 8.22 to 42.7 Day5 (CR) Paired vs Unpaired $p > 0.999$; 95% CI: 13.4 to 47.9 Paired vs neutral $p < 0.001$; 95% CI: -15.7 to 18.8 Day6 (RT-PP) Paired vs Unpaired $p > 0.999$; 95% CI: -18.2 to 16.2 Paired vs neutral $p < 0.001$; 95% CI: 13.0 to 47.5 Day7 (RT-PP) Paired vs Unpaired $p < 0.001$; 95% CI: -17.6 to 16.9 Paired vs neutral $p > 0.999$; 95% CI: 10.8 to 45.2 Day8 (CR) Paired vs Unpaired $p < 0.001$; 95% CI: -13.1 to 21.3

				<p>Paired vs neutral $p > 0.999$; 95% CI: 7.45 to 41.9</p> <p>Reversal parameters: Day3 paired vs Day6 unpaired $p = 0.991$; 95% CI: -24.6 to 9.91 Day3 paired vs Day7 unpaired $p = 0.995$; 95% CI: -24.2 to 10.2 Day4 paired vs Day6 unpaired $p > 0.999$; 95% CI: -19.5 to 15.0 Day4 paired vs Day7 unpaired $p > 0.999$; 95% CI: -19.1 to 15.3 Day5 paired vs Day8 unpaired $p > 0.999$; 95% CI: -17.2 to 17.3</p>
<p>Figure 8D (right) time spent in paired, unpaired and neutral compartments during the 4 RT-PP days for Calb2-Cre/Chr2 mice</p>	Normally distributed	RM One-Way ANOVA followed by Tukey's multiple comparison test	N=7 (M=0, F=7)	<p>Compartment $p < 0.001$, $F_{(2,6)} = 90.1$</p> <p>Multiple comparisons Paired vs unpaired $p = 0.297$; 95% CI: -11.4 to 3.42 Paired vs neutral $p < 0.001$; 95% CI: 18.5 to 33.3 Unpaired vs neutral $p < 0.001$; 95% CI: 22.4 to 37.3</p>
<p>Figure 8-1F Behavioral analysis of Calb2-Cre/Chr2 mice tested on high power, throughout the opto-behavioral experiments</p>	Normally distributed	Two-way RM ANOVA followed by Tukey's multiple comparison test	N=7 (M=0, F=7)	<p>Interaction: $p = 0.927$, $F_{(12,72)} = 0.469$ Day: $p = 0.661$, $F_{(6,36)} = 0.688$ Compartment: $p = 0.001$, $F_{(2,12)} = 12.5$</p> <p>Multiple comparisons (of interest) Day2 (Pre-test) Paired vs Unpaired $p = 0.104$; 95% CI: -33.5 to 1.28 Day3 (RT-PP) Paired vs Unpaired $p = 0.995$; 95% CI: -24.4 to 10.4 Paired vs neutral $p = 0.019$; 95% CI: 1.56 to 36.3 Day4 (RT-PP) Paired vs Unpaired $p > 0.999$; 95% CI: -22.6 to 12.2 Paired vs neutral $p < 0.001$; 95% CI: 47.1 to 119 Day5 (CR) Paired vs Unpaired $p = 0.742$; 95% CI: -28.2 to 6.54 Paired vs neutral $p = 0.015$; 95% CI: 1.87 to 36.6 Day6 (RT-PP) Paired vs Unpaired $p = 0.937$; 95% CI: -26.3 to 8.46 Paired vs neutral $p < 0.001$; 95% CI: 11.1 to 45.9 Day7 (RT-PP) Paired vs Unpaired $p > 0.999$; 95% CI: -22.3 to 12.5 Paired vs neutral $p < 0.001$; 95% CI: 7.32 to 42.1 Day8 (CR) Paired vs Unpaired $p = 0.976$; 95% CI: -25.5 to 9.30 Paired vs neutral $p < 0.001$; 95% CI: 7.52 to 42.3</p> <p>Reversal parameters: Day3 paired vs Day6 unpaired $p > 0.999$; 95% CI: -17.0 to 17.8 Day3 paired vs Day7 unpaired $p > 0.999$; 95% CI: -18.4 to 16.4 Day4 paired vs Day6 unpaired $p > 0.999$; 95% CI: -15.1 to 19.6 Day4 paired vs Day7 unpaired $p > 0.999$; 95% CI: -16.5 to 18.2 Day5 paired vs Day8 unpaired $p > 0.999$; 95% CI: -17.5 to 17.3</p>
<p>Figure 8-1F (right) time spent in paired, unpaired and neutral compartments during the 4 RT-PP days for Calb2-Cre/Chr2 mice under high power stimulation</p>	Normally distributed	RM One-Way ANOVA followed by Tukey's multiple comparison test	N=7 (M=0, F=7)	<p>Compartment $p < 0.001$, $F_{(2,6)} = 47.3$</p> <p>Multiple comparisons Paired vs unpaired $p = 0.988$; 95% CI: -8.15 to 8.97 Paired vs neutral $p < 0.001$; 95% CI: 15.1 to 32.3 Unpaired vs neutral $p < 0.001$; 95% CI: 14.7 to 31.8</p>
<p>Figure 8E (left) Behavioral analysis of NEX-Cre/Chr2 mice throughout the opto-behavioral experiments</p>	Normally distributed	Two-way RM ANOVA followed by Tukey's multiple comparison test	N=5 (M=1, F=4)	<p>Interaction: $p < 0.001$, $F_{(12,48)} = 4.63$ Day: $p = 0.307$, $F_{(6,24)} = 1.27$ Compartment: $p < 0.001$, $F_{(2,8)} = 76.8$</p> <p>Multiple comparisons (of interest) Day2 (Pre-test) Paired vs Unpaired $p > 0.999$; 95% CI: -18.7 to 24.9 Day3 (RT-PP) Paired vs Unpaired $p = 0.414$; 95% CI: -5.70 to 37.9 Paired vs neutral $p < 0.001$; 95% CI: 17.1 to 60.7 Day4 (RT-PP) Paired vs Unpaired $p > 0.999$; 95% CI: -17.5 to 26.1 Paired vs neutral $p < 0.001$; 95% CI: 16.6 to 60.3 Day5 (CR) Paired vs Unpaired $p > 0.999$; 95% CI: 12.0 to 55.6</p>

				<p>Paired vs neutral $p < 0.001$; 95% CI: -5.03 to 38.6</p> <p>Day6 (RT-PP)</p> <p>Paired vs Unpaired $p = 0.020$; 95% CI: -45.5 to -1.92</p> <p>Paired vs neutral $p < 0.001$; 95% CI: 15.1 to 58.7</p> <p>Day7 (RT-PP)</p> <p>Paired vs Unpaired $p < 0.001$; 95% CI: -51.8 to -8.16</p> <p>Paired vs neutral $p < 0.001$; 95% CI: 20.5 to 64.1</p> <p>Day8 (CR)</p> <p>Paired vs Unpaired $p = 0.937$; 95% CI: -32.7 to 10.9</p> <p>Paired vs neutral $p < 0.001$; 95% CI: 16.3 to 59.9</p> <p>Reversal parameters:</p> <p>Day3 paired vs Day6 unpaired $p = 0.049$; 95% CI: 0.0239 to 43.6</p> <p>Day3 paired vs Day7 unpaired $p = 0.016$; 95% CI: 2.38 to 46.0</p> <p>Day4 paired vs Day6 unpaired $p = 0.252$; 95% CI: -4.06 to 39.5</p> <p>Day4 paired vs Day7 unpaired $p = 0.105$; 95% CI: -1.71 to 41.9</p> <p>Day5 paired vs Day8 unpaired $p = 0.998$; 95% CI: -14.0 to 29.6</p>
<p>Figure 8E (right) time spent in paired, unpaired and neutral compartments during the 4 RT-PP days for NEX-Cre/Chr2 mice</p>	Normally distributed	RM One-Way ANOVA followed by Tukey's multiple comparison test	N=5 (M=1, F=4)	<p>Compartment $p < 0.001$, $F_{(2,6)} = 39.7$</p> <p>Multiple comparisons</p> <p>Paired vs unpaired $p = 0.013$; 95% CI: 5.03 to 32.0</p> <p>Paired vs neutral $p < 0.001$; 95% CI: 25.7 to 52.6</p> <p>Unpaired vs neutral $p = 0.008$; 95% CI: 7.16 to 34.1</p>
<p>Figure 8-1G (left) Behavioral analysis of NEX-Cre/Chr2 mice tested on high power, throughout the opto-behavioral experiments</p>	Normally distributed	Two-way RM ANOVA followed by Tukey's multiple comparison test	N=4 (M=1, F=3)	<p>Interaction: $p < 0.001$, $F_{(12,36)} = 8.58$</p> <p>Day: $p = 0.252$, $F_{(6,18)} = 1.44$</p> <p>Compartment: $p < 0.001$, $F_{(2,6)} = 48.3$</p> <p>Multiple comparisons (of interest)</p> <p>Day2 (Pre-test)</p> <p>Paired vs Unpaired $p = 0.369$; 95% CI: -25.0 to 3.62</p> <p>Day3 (RT-PP)</p> <p>Paired vs Unpaired $p = 0.358$; 95% CI: -3.54 to 25.1</p> <p>Paired vs neutral $p < 0.001$; 95% CI: 16.0 to 44.6</p> <p>Day4 (RT-PP)</p> <p>Paired vs Unpaired $p = 0.003$; 95% CI: 3.97 to 32.6</p> <p>Paired vs neutral $p < 0.001$; 95% CI: 24.9 to 53.5</p> <p>Day5 (CR)</p> <p>Paired vs Unpaired $p = 0.084$; 95% CI: -0.819 to 27.8</p> <p>Paired vs neutral $p < 0.001$; 95% CI: 19.7 to 48.3</p> <p>Day6 (RT-PP)</p> <p>Paired vs Unpaired $p = 0.087$; 95% CI: -27.8 to 0.877</p> <p>Paired vs neutral $p < 0.001$; 95% CI: 17.7 to 46.4</p> <p>Day7 (RT-PP)</p> <p>Paired vs Unpaired $p < 0.001$; 95% CI: -34.7 to -6.03</p> <p>Paired vs neutral $p < 0.001$; 95% CI: 21.8 to 50.5</p> <p>Day8 (CR)</p> <p>Paired vs Unpaired $p = 0.798$; 95% CI: -22.5 to 6.11</p> <p>Paired vs neutral $p < 0.001$; 95% CI: 13.7 to 42.3</p> <p>Reversal parameters:</p> <p>Day3 paired vs Day6 unpaired $p = 0.203$; 95% CI: -2.36 to 26.3</p> <p>Day3 paired vs Day7 unpaired $p = 0.028$; 95% CI: 0.881 to 29.5</p> <p>Day4 paired vs Day6 unpaired $p = 0.005$; 95% CI: 3.12 to 31.8</p> <p>Day4 paired vs Day7 unpaired $p < 0.001$; 95% CI: 6.36 to 35.0</p> <p>Day5 paired vs Day8 unpaired $p = 0.202$; 95% CI: -2.35 to 26.3</p>
<p>Figure 8-1G (right) time spent in paired, unpaired and neutral compartments during the 4 RT-PP days for NEX-Cre/Chr2 mice under high power stimulation</p>	Normally distributed	RM One-Way ANOVA followed by Tukey's multiple comparison test	N=4 (M=1, F=3)	<p>Compartment $p < 0.001$, $F_{(2,6)} = 178$</p> <p>Multiple comparisons</p> <p>Paired vs unpaired $p < 0.001$; 95% CI: 10.1 to 21.3</p> <p>Paired vs neutral $p < 0.001$; 95% CI: 28.8 to 40.0</p> <p>Unpaired vs neutral $p < 0.001$; 95% CI: 13.1 to 24.3</p>
<p>Figure 8-1H (left) Behavioral analysis of bilaterally injected NEX-Cre/Chr2 mice throughout the opto-</p>	Normally distributed	Two-way RM ANOVA followed by Tukey's multiple	N=4 (M=0, F=4)	<p>Interaction: $p = 0.040$, $F_{(12,36)} = 2.13$</p> <p>Day: $p = 0.384$, $F_{(6,18)} = 1.13$</p> <p>Compartment: $p < 0.001$, $F_{(2,6)} = 43.3$</p> <p>Multiple comparisons (of interest)</p>

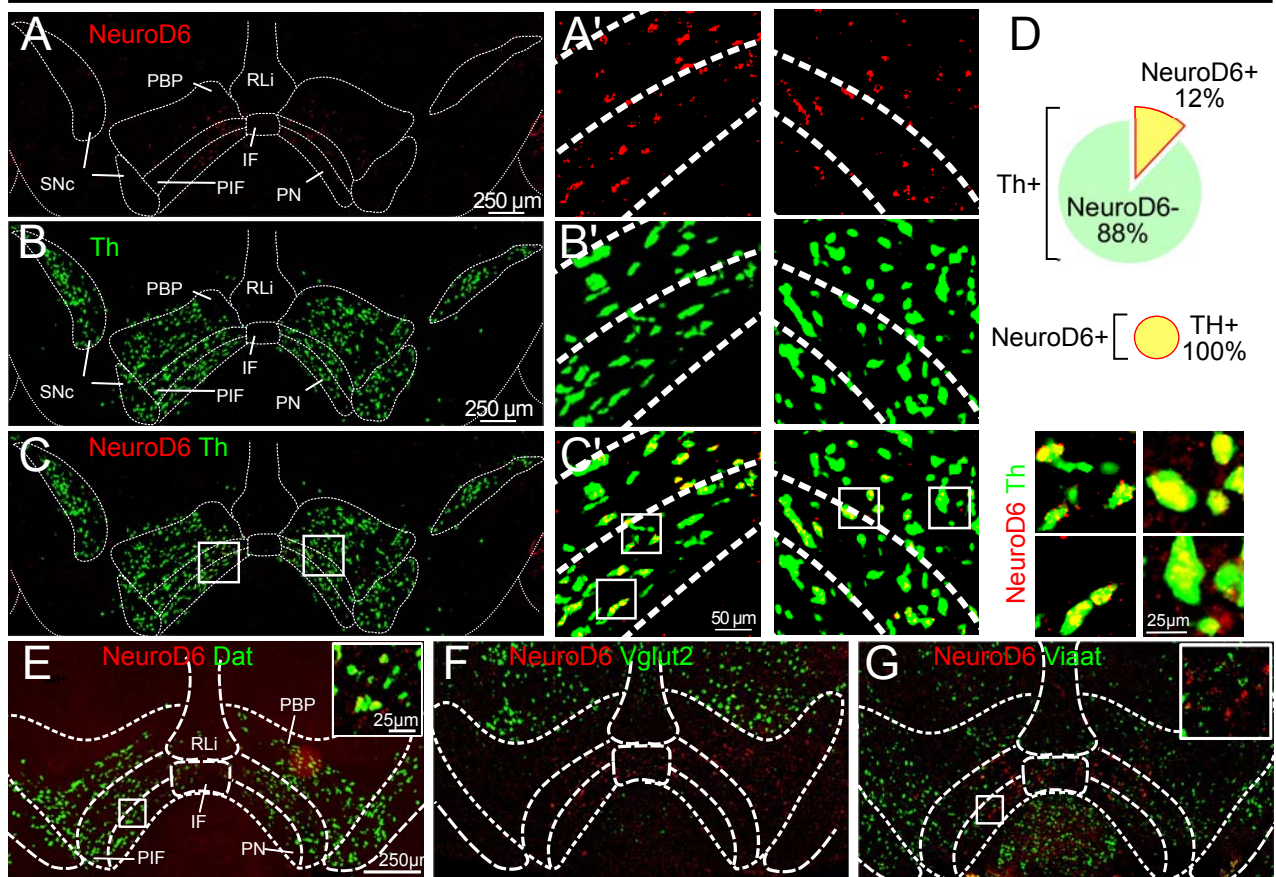
behavioral experiments		comparison test		<p>Day2 (Pre-test) Paired vs Unpaired $p=0.999$; 95% CI: -50.7 to 25.1 Day3 (RT-PP) Paired vs Unpaired $p=0.998$; 95% CI: -24.6 to 51.2 Paired vs neutral $p=0.017$; 95% CI: 4.27 to 80.1 Day4 (RT-PP) Paired vs Unpaired $p=0.768$; 95% CI: -15.7 to 60.2 Paired vs neutral $p=0.003$; 95% CI: 10.3 to 86.1 Day5 (CR) Paired vs Unpaired $p=0.974$; 95% CI: -21.2 to 54.7 Paired vs neutral $p=0.015$; 95% CI: 4.63 to 80.5 Day6 (RT-PP) Paired vs Unpaired $p>0.999$; 95% CI: -49.6 to 26.3 Paired vs neutral $p=0.029$; 95% CI: 2.13 to 78.0 Day7 (RT-PP) Paired vs Unpaired $p=0.999$; 95% CI: -52.5 to 23.3 Paired vs neutral $p=0.019$; 95% CI: 3.69 to 79.5 Day8 (CR) Paired vs Unpaired $p=0.185$; 95% CI: -70.1 to 5.78 Paired vs neutral $p<0.001$; 95% CI: 14.2 to 90.0 Reversal parameters: Day3 paired vs Day6 unpaired $p=0.999$; 95% CI: -25.0 to 50.8 Day3 paired vs Day7 unpaired $p=0.995$; 95% CI: -23.6 to 52.3 Day4 paired vs Day6 unpaired $p=0.952$; 95% CI: -20.0 to 55.8 Day4 paired vs Day7 unpaired $p=0.999$; 95% CI: -18.6 to 57.3 Day5 paired vs Day8 unpaired $p=0.668$; 95% CI: -14.1 to 61.8</p>
Figure 8-1H (right) time spent in paired, unpaired and neutral compartments during the 4 RT-PP days for bilaterally injected NEX-Cre/Chr2 mice	Normally distributed	RM One-Way ANOVA followed by Tukey's multiple comparison test	N=4 (M=0, F=4)	<p>Compartment $p < 0.001$, $F_{(2,6)} = 331$ Multiple comparisons Paired vs unpaired $p<0.001$; 95% CI: 10.1 to 20.8 Paired vs neutral $p<0.001$; 95% CI: 37.7 to 48.4 Unpaired vs neutral $p<0.001$; 95% CI: 22.2 to 32.9</p>
Figure 8F (left) Behavioral analysis of bilaterally injected NEX-Cre/Chr2 mice throughout the opto-behavioral experiments, tested on high power	Normally distributed	Two-way RM ANOVA followed by Tukey's multiple comparison test	N=4 (M=0, F=4)	<p>Interaction: $p < 0.001$, $F_{(12,36)} = 9.03$ Day: $p = 0.310$, $F_{(6,18)} = 1.29$ Compartment: $p < 0.001$, $F_{(2,6)} = 36.5$ Multiple comparisons (of interest) Day2 (Pre-test) Paired vs Unpaired $p=0.982$; 95% CI: -42.9 to 17.4 Day3 (RT-PP) Paired vs Unpaired $p=0.349$; 95% CI: -7.34 to 53.0 Paired vs neutral $p<0.001$; 95% CI: 20.0 to 80.3 Day4 (RT-PP) Paired vs Unpaired $p<0.001$; 95% CI: 14.1 to 74.4 Paired vs neutral $p<0.001$; 95% CI: 30.8 to 91.1 Day5 (CR) Paired vs Unpaired $p>0.999$; 95% CI: -29.7 to 30.6 Paired vs neutral $p=0.002$; 95% CI: 9.24 to 69.5 Day6 (RT-PP) Paired vs Unpaired $p<0.001$; 95% CI: -76.1 to -15.8 Paired vs neutral $p<0.001$; 95% CI: 28.5 to 88.8 Day7 (RT-PP) Paired vs Unpaired $p<0.001$; 95% CI: -74.4 to -14.1 Paired vs neutral $p<0.001$; 95% CI: 27.0 to 87.3 Day8 (CR) Paired vs Unpaired $p=0.989$; 95% CI: -42.4 to 17.9 Paired vs neutral $p=0.006$; 95% CI: 6.19 to 66.5 Reversal parameters: Day3 paired vs Day6 unpaired $p=0.009$; 95% CI: 5.24 to 65.5 Day3 paired vs Day7 unpaired $p=0.011$; 95% CI: 4.65 to 64.9 Day4 paired vs Day6 unpaired $p<0.001$; 95% CI: 16.0 to 76.3 Day4 paired vs Day7 unpaired $p<0.001$; 95% CI: 15.4 to 75.7 Day5 paired vs Day8 unpaired $p>0.999$; 95% CI: -20.8 to 39.5</p>
Figure 8F (right) time spent in	Assumed	RM One-Way	N=4	Compartment $p < 0.001$, $F_{(2,6)} = 106$

paired, unpaired and neutral compartments during the 4 RT-PP days for NEX-Cre/ChR2 mice bilaterally injected and under high power stimulation	normality	ANOVA followed by Tukey's multiple comparison test	(M=0, F=4)	Multiple comparisons Paired vs unpaired $p < 0.001$; 95% CI: 27.1 to 51.6 Paired vs neutral $p < 0.001$; 95% CI: 44.5 to 69.0 Unpaired vs neutral $p = 0.011$; 95% CI: 5.19 to 29.7
Figure 8-11ii Behavioral analysis of Vglut2-Cre throughout the NCP experiments	Normally distributed	RM One-Way ANOVA followed by Tukey's multiple comparison test	N=5 (M=0, F=5)	Interaction: $p = 0.002$, $F_{(4,16)} = 6.90$ Day: $p = 0.410$, $F_{(2,8)} = 1$ Compartment: $p < 0.001$, $F_{(2,8)} = 70.9$ Multiple comparisons (of interest) Stimulation 1 Neutral vs Paired1 $p = 0.009$; 95% CI: -93.5 to -10.6 Neutral vs Paired2 $p = 0.004$; 95% CI: -98.6 to -15.7 Paired 1 vs Paired2 $p > 0.999$; 95% CI: -36.4 to 46.5 Stimulation 2 Neutral vs Paired1 $p < 0.001$; 95% CI: -113 to -29.9 Neutral vs Paired2 $p < 0.001$; 95% CI: -112 to -29. Paired 1 vs Paired2 $p > 0.999$; 95% CI: -42.3 to 40.6 CR Neutral vs Paired1 $p = 0.998$; 95% CI: -49.8 to 33.1 Neutral vs Paired2 $p > 0.999$; 95% CI: -35.5 to 47.4 Paired 1 vs Paired2 $p = 0.938$; 95% CI: -55.7 to 27.2
Figure 8-11iii time spent in paired1, paired2 and neutral compartments during the 2 NCP days for Vglut2-Cre/ChR2 mice	Normally distributed	RM One-Way ANOVA followed by Tukey's multiple comparison test	N=5 (M=0, F=5)	Compartment $p = 0.018$, $F_{(2,2)} = 54.2$ Multiple comparisons Paired1 vs Paired2 $p = 0.951$; 95% CI: -38.9 to 43.2 Paired1 vs Neutral $p = 0.023$; 95% CI: -103 to -20.7 Paired2 vs Neutral $p = 0.021$; 95% CI: -105 to -22.8

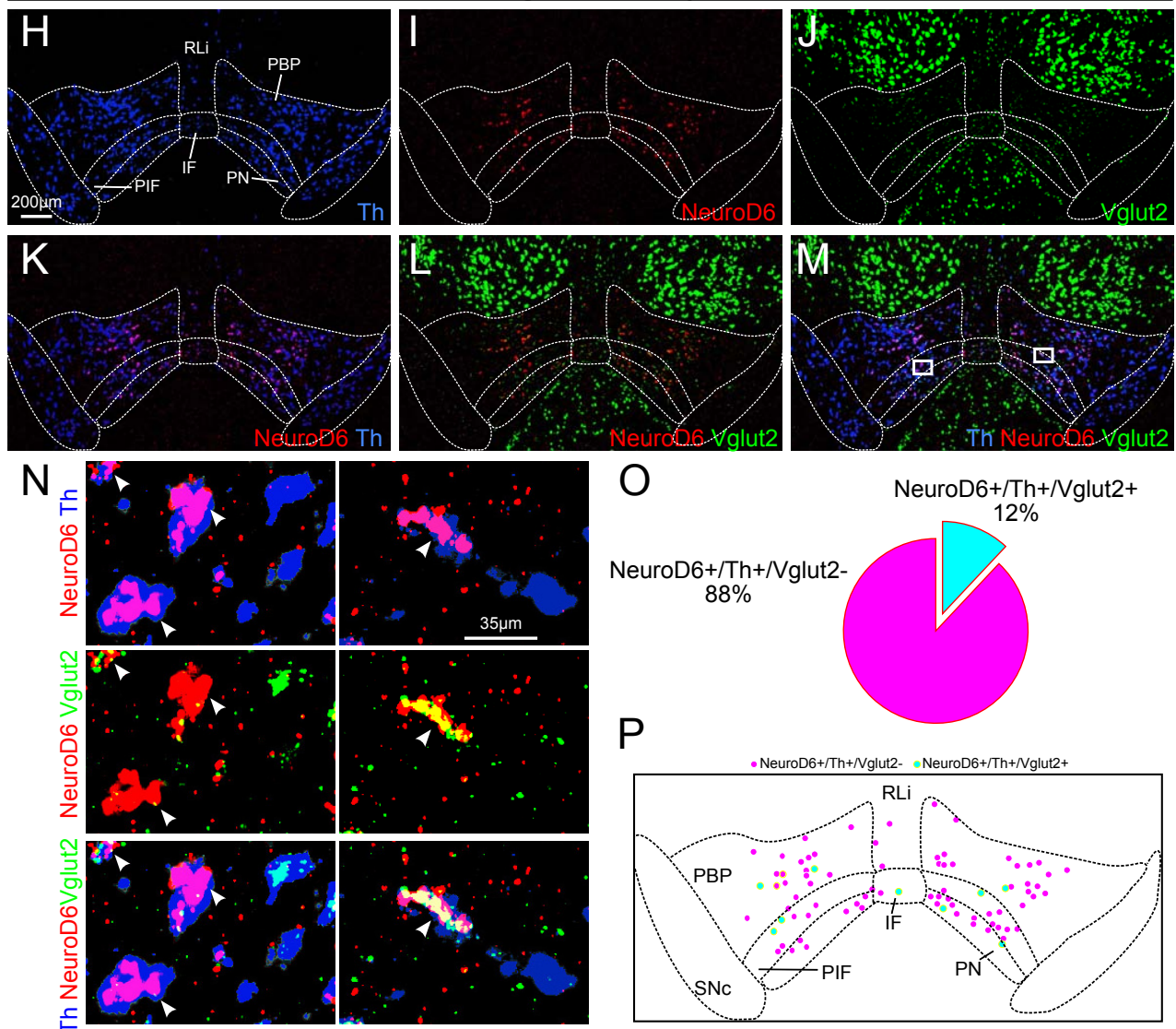
Table 2

Area	Cre-driver			
	DAT	Vglut2	Calb2	NEX
Anterior olfactory area	+	+	+	+
Medial prefrontal cortex (infralimbic, prelimbic, and anterior cingulate cortices)	+	+	+	+
(Medial) orbital cortex	+	+	+	+
Nucleus accumbens shell	+	+	(+)	+
Nucleus accumbens core	+	-	-	+
Dorsomedial Striatum	+	-	-	-
Olfactory tubercle	+	+	+	+
Cingulate cortex	+	+	+	+
Septum/septal nuclei	+	+	-	+
Diagonal band of Broca	+	+	+	+
Ventral pallidum	+	+	+	+
Bed nuclei of the stria terminalis	+	+	+	+
Preoptic area	+	+	+	+
Lateral habenula	+	+	-	-
Medial habenula	-	-	+	+
Hippocampus	-	-	-	+
Dentate gyrus	-	-	-	+
Amygdala	+	+	+	+
Hypothalamic area	+	+	-	+

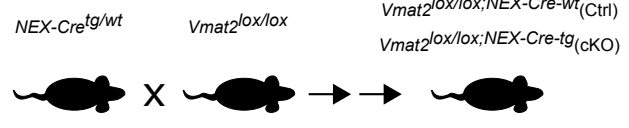
Double labeling *in situ* hybridization



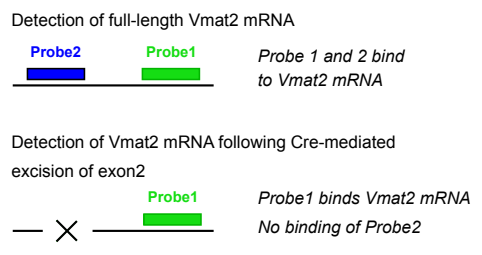
Triple labeling *in situ* hybridization



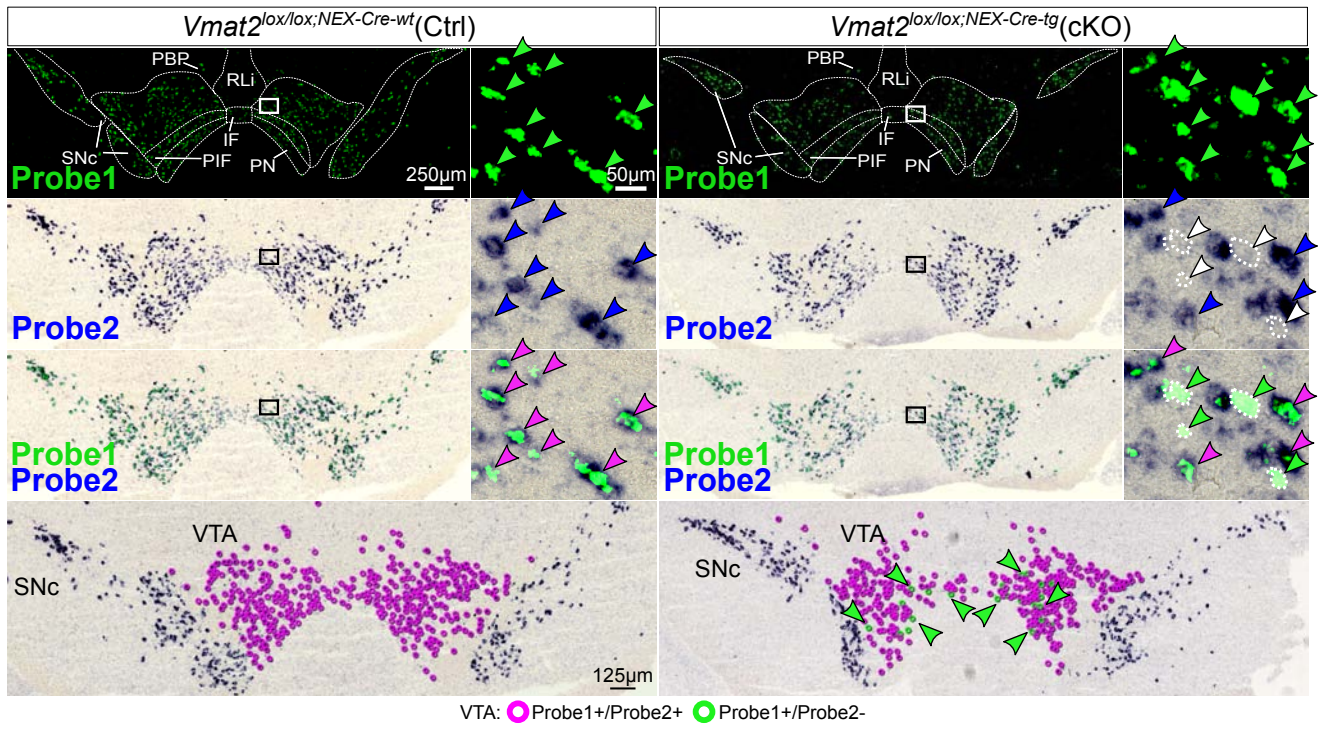
A NeuroD6-mediated targeting of Vmat2



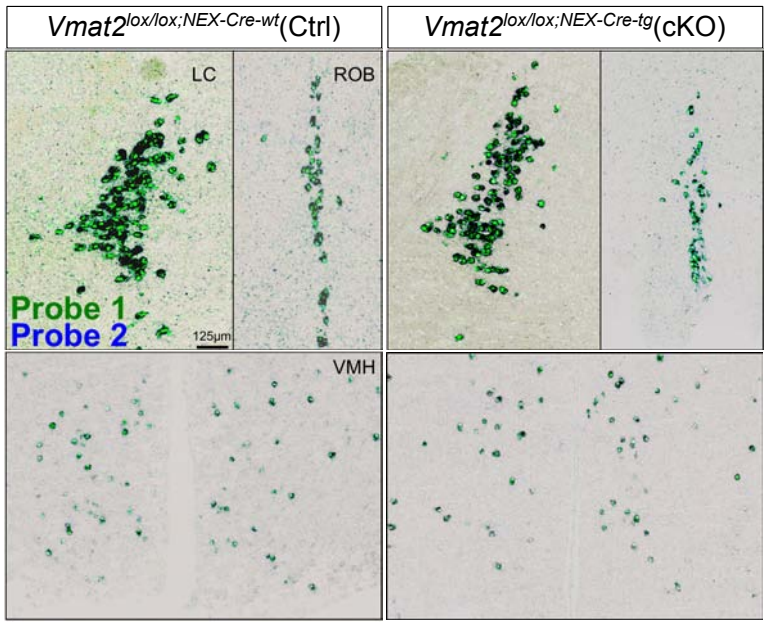
B Vmat2 mRNA 2-probe approach



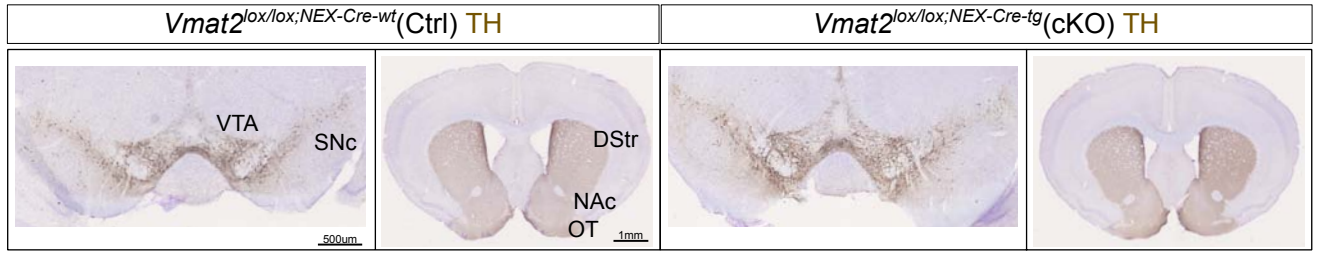
C



D



E



○ □ *Vmat2^{lox/lox};NEX-Cre-wt*(Ctrl) ● ■ *Vmat2^{lox/lox};NEX-Cre-tg*(cKO)

